



**HAL**  
open science

# Direct introduction MALDI FTICR MS based on dried droplet deposition applied to non-targeted metabolomics on *Pisum Sativum* root exudates

Valentina Calabrese, Isabelle Schmitz-Afonso, Wassila Riah-Anglet, Isabelle Trinsoutrot-Gattin, Barbara Pawlak, Carlos Afonso

## ► To cite this version:

Valentina Calabrese, Isabelle Schmitz-Afonso, Wassila Riah-Anglet, Isabelle Trinsoutrot-Gattin, Barbara Pawlak, et al.. Direct introduction MALDI FTICR MS based on dried droplet deposition applied to non-targeted metabolomics on *Pisum Sativum* root exudates. *Talanta*, 2023, 253, pp.123901. 10.1016/j.talanta.2022.123901 . hal-04027945

**HAL Id: hal-04027945**

**<https://normandie-univ.hal.science/hal-04027945v1>**

Submitted on 30 Oct 2024

**HAL** is a multi-disciplinary open access archive for the deposit and dissemination of scientific research documents, whether they are published or not. The documents may come from teaching and research institutions in France or abroad, or from public or private research centers.

L'archive ouverte pluridisciplinaire **HAL**, est destinée au dépôt et à la diffusion de documents scientifiques de niveau recherche, publiés ou non, émanant des établissements d'enseignement et de recherche français ou étrangers, des laboratoires publics ou privés.

1 **Direct Introduction MALDI FTICR MS based on dried droplet deposition**  
2 **applied to non-targeted metabolomics on *Pisum Sativum* Root Exudates**

3

4 **Valentina Calabrese <sup>a</sup>, Isabelle Schmitz-Afonso <sup>a,\*</sup>, Wassila Riah-Anglet <sup>b</sup>, Isabelle**  
5 **Trinsoutrot-Gattin <sup>b</sup>, Barbara Pawlak <sup>c</sup>, Carlos Afonso <sup>a</sup>**

6 <sup>a</sup> Normandie Univ, COBRA, UMR 6014 and FR 3038, Université de Rouen, INSA de Rouen,  
7 CNRS, IRCOF, 1 rue Tesnières, 76821 Mont-Saint-Aignan, Cedex, France.

8 <sup>b</sup> UniLaSalle, AGHYLE Research Unit UP 2018.C101, Rouen Team, 76134 Mont-Saint  
9 Aignan, SFR Normandie Végétal FED 4277, 76000 Rouen, France.

10 <sup>c</sup> Laboratoire GlycoMEV UR 4358, Université de Rouen Normandie, SFR Normandie  
11 Végétal FED 4277, 76000 Rouen, France

12

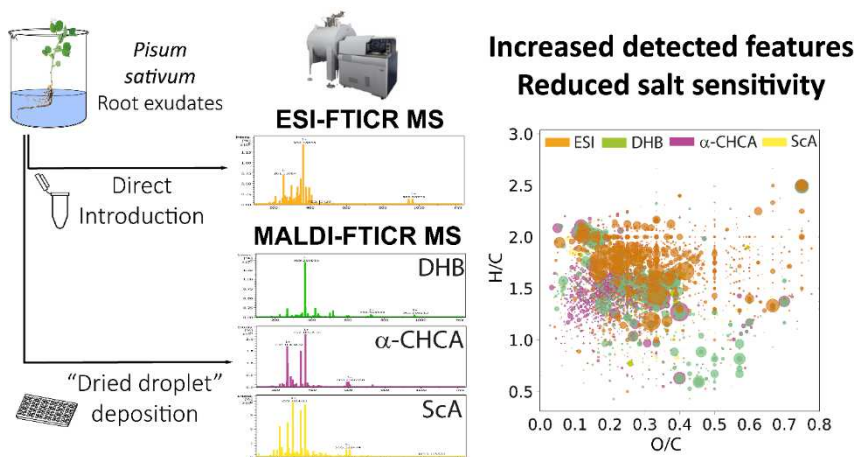
13 \*Corresponding author at : Normandie Univ, COBRA, UMR 6014 and FR 3038, Université  
14 de Rouen, INSA de Rouen, CNRS, IRCOF, 1 rue Tesnières, 76821 Mont-Saint-Aignan,  
15 Cedex, France. E-mail address : isabelle.schmitz-afonso@univ-rouen.fr

16

17 **Key words** Root exudates, Non-targeted metabolomics, Fourier Transform Ion Cyclotron  
18 Resonance Mass Spectrometry, MALDI, *Pisum sativum*

19

20 **Graphical abstract**



21

## 22 **Abstract**

23 Non-targeted metabolomic approaches based on direct introduction (DI) through a soft  
24 ionization source are nowadays used for large-scale analysis and wide cover-up of metabolites  
25 in complex matrices. When coupled with ultra-high-resolution Fourier-Transform ion  
26 cyclotron resonance (FTICR MS), DI is generally performed through electrospray (ESI),  
27 which, despite the great analytical throughput, can suffer of matrix effects due to residual salts  
28 or charge competitors. In alternative, matrix assisted laser desorption ionization (MALDI)  
29 coupled with FTICR MS offers relatively high salt tolerance but it is mainly used for imaging  
30 of small molecule within biological tissues. In this study, we report a systematic evaluation on  
31 the performance of direct introduction ESI and MALDI coupled with FTICR MS applied to  
32 the analysis of root exudates (RE), a complex mixture of metabolites released from plant root  
33 tips and containing a relatively high salt concentration. Classic dried droplet deposition  
34 followed by screening of best matrices and ratio allowed the selection of high ranked  
35 conditions for non-targeted metabolomics on RE. Optimization of MALDI parameters led to  
36 improved reproducibility and precision. A RE desalted sample was used for comparison on  
37 ionization efficiency of the two sources and ion enhancement at high salinity was highlighted  
38 in MALDI by spiking desalted solution with inorganic salts. Application of a true lyophilized  
39 RE sample exhibited the complementarity of the two sources and the ability of MALDI in the  
40 detection of undisclosed metabolites suffering of matrix effects in ESI mode.

41

## 42 **1. Introduction**

43 Non-targeted metabolomics is a growing field of ‘omics’ which enables the unbiased  
44 detection and annotation of a wide range of molecules at low molecular weight (< 1500 Da) in  
45 biological samples [1–6]. In the case of plant science, metabolite profiling could give access  
46 to the characterization of primary and secondary metabolites which are widely involved in  
47 plant growth, development and health or adaptation to abiotic and biotic stress. It could be  
48 drought, extremes temperatures, salinity or attack by pathogenic microorganisms [7–13].  
49 Non-targeted metabolomic is typically performed through nuclear magnetic resonance (NMR)  
50 [14,15] and mass spectrometry (MS) [16]. Over the past decades, MS coupled with gas (GC-  
51 MS) [17] or liquid chromatography (LC-MS) [18] has been widely used as preferred  
52 technique for the detection of a wide range of compounds in plant material. In the case of  
53 complex matrices, LC-MS allows the separation of isomeric and isobaric species before their

54 detection as ions in gas-phase [19]. Chromatographic separation allows a reduction of sample  
55 complexity but it is a highly time-consuming technique and it presents some limitations in  
56 large-scale non-targeted metabolomic studies [20]. Recently, non-targeted metabolomic  
57 approaches based on the direct introduction (DI) of the sample into the ion source have been  
58 proved to enable faster analysis for large-scale study and wide cover-up of metabolite  
59 detection [21,22]. Among these, direct introduction coupled with ultra-high-resolution  
60 analyzers as in Fourier Transform ion cyclotron resonance mass spectrometry (FTICR MS)  
61 [23,24] has been increasingly used in non-targeted metabolomic thanks to its advantages in  
62 ultra-high resolving power, high mass accuracy and dynamic range [25–28]. Recently, many  
63 studies have been published on the potentiality of FTICR MS to perform a global profiling of  
64 metabolites in plants material [27–31]. FTICR analyzers enable separation according to the  
65 cyclotron frequency produced by the rotation of ions in a fixed magnetic field and the  
66 simultaneous detection of all  $m/z$  over a time range [32]. In this extent, when coupled with  
67 FTICR MS, direct introduction allows to obtain a constant number of ions entering into the  
68 ICR cell during wide time ranges, leading to ultra-high resolution and mass measure  
69 precision. For this reason, direct introduction FTICR MS is normally preferred over  
70 hyphenation with liquid chromatography. Direct introduction FTICR MS coupled with  
71 electrospray (ESI) is routinely used as preferred source in non-targeted metabolomic studies  
72 because it enables the easy and efficient ionization of a wide range of metabolites  
73 characterizing many biological matrices [33–35]. However, ESI suffers from some analytical  
74 limitations as matrix effects [36]. In fact, when a wide number of different analytes is injected  
75 in the source, ions might compete as charge carriers (ion competition) or species at high  
76 abundance can lead to reduced sensitivity of low abundance ones (ion suppression) [37–39].  
77 Matrix assisted laser desorption ionization (MALDI) is an alternative ion source which  
78 enables the soft ionization of a wide range of metabolites in biological samples [40]. This is  
79 normally performed through the use of an organic matrix which assists the transfer of the laser  
80 energy to the analyte, enabling the ionization and reducing ion fragmentation. MALDI  
81 enables the performant detection of metabolites in complex biological samples without  
82 preliminary clean-up or separation before analysis. However, when coupled with classical  
83 mass analyzers such as time of flights, the presence of matrix ions in the low  $m/z$  zone limits  
84 its applications in the analysis of low molecular weight compounds [41]. MALDI has  
85 therefore been applied mostly in the analysis of large organic biomolecules such as lipids and  
86 proteins[42,43], peptides [44,45] and saccharides [46] or in whole-cell samples analysis for  
87 the detection of intact microorganisms [47]. Lately, coupling with FTICR MS has boosted

88 application of MALDI in low molecular weight compounds discovery thanks to improved  
89 molecular formula assignment for isobaric ions [48,49]. Nonetheless, MALDI-FTICR MS is  
90 nowadays mainly used in metabolomics to highlight the spatial distribution of a reduced  
91 number of compounds within biological tissues [50,51]. Many studies point out on imaging  
92 for biomedical applications or in plant science [52–58]. Nonetheless, to the best of our  
93 knowledge, few studies points out on a non-targeted metabolomic approach based on the  
94 direct introduction of a biological sample based on MALDI-FTICR MS [59]. In fact, the  
95 highest drawback of mass spectrometry based on MALDI is that, besides from problems  
96 connected to the noise in the low mass region [60], ionization depends strictly on the  
97 homogeneity of the matrix-sample spot [61]. This can lead to issues as lack of reproducibility  
98 for qualitative and mostly quantitative analysis [62].

99 In this study we present for the first time an analytical optimization of a non-targeted  
100 metabolomic approach based on ultra-high-resolution mass spectrometry coupled to direct  
101 introduction MALDI for improved metabolite detection and reduced ion suppression in  
102 presence of salts. This method has been optimized on plant root exudates (RE), because this  
103 complex biological cocktail contains a high number and diversity of molecules and residual  
104 salts [11]. Indeed, RE is a mixture of primary and secondary metabolites produced by the  
105 plant roots and continuously released into the narrow zone of soil surrounding roots called the  
106 rhizosphere [12]. These include many compounds of different nature which take a large part  
107 in the interactions between plants and their environment [63,64], especially with the  
108 rhizosphere microbiota essential to plant growth, health and resistance to biotic or abiotic  
109 stress [12,64–67]. Deciphering molecular signals exchanged between the root and its  
110 microbiota would be an important advancement in plant science and a great hope for  
111 agroecology, because a better control of interactions in the rhizosphere could allow limitation  
112 of phytochemical inputs in agricultural processes [68]. These objectives could be reached  
113 through the metabolomic investigation and profiling of plant RE [11,69]. Nonetheless, due to  
114 the complexity of RE composition and its variability with plant growth conditions and variety,  
115 performing metabolomic studies of root exudates is challenging and many efforts are required  
116 for the optimization of both RE collection [70] and analysis through mass spectrometry  
117 techniques [71]. RE sampling is usually divided in two steps consisting in plant growth and  
118 metabolite extraction [72]. Among many plant growth methods, artificial hydroponic systems  
119 are widely used as they enable an easier handling of plants and improved reproducibility with  
120 low root damage and reduced metabolites absorption from matrix [70,73]. In hydroponics,  
121 plant growth is obtained through immersion of seeds and roots in a nutritive medium

122 containing macronutrient [74]. Once growth completed, RE can be collected by rinsing, then  
123 transferring the root system from the hydroponic medium to a solvent that is compatible with  
124 analysis (i.e. water) [75,76]. It is worth to note that, in RE samples obtained from hydroponic  
125 systems, metabolites occur at mM–nM concentrations; while a relatively high concentration  
126 of macronutrients (mM) may be present after re-concentration of RE samples [77]. Therefore,  
127 in the case of mass spectrometry-based metabolomics coupled with direct introduction,  
128 metabolite extraction and salt removal are highly advised to obtain the preferential ionization  
129 of the metabolites over suppression and competition effects [71].

130 Here, we evaluated the performances of MALDI-FTICR MS based on dried droplet  
131 deposition to a non-targeted metabolomic approach for the detection and annotation of low  
132 abundance metabolites in *Pisum sativum* RE. Literature presents many studies on *P. sativum*  
133 RE showing the presence of amino acids, sugars and organic acids [78], while few  
134 investigations focus on the isolation and characterization of secondary metabolites. The main  
135 chemical classes have been found to be triterpenes [79], polyphenols [80,81], alkaloids [82]  
136 and some classes of specialized phytohormones [83–85]. Nonetheless, to the best of our  
137 knowledge, this is the first non-targeted metabolomic study on *P. sativum* RE. In this study, a  
138 *P. sativum* RE desalted sample was first submitted to a classic non-targeted metabolomic  
139 approach based on data dependent acquisition mass spectrometry (DDA-MS) and to ESI-  
140 FTICR MS. A collection of 48 metabolites were annotated with a hypothetical structure and a  
141 global profiling with an insight of different chemical classes was obtained *via* unique  
142 molecular formula assignment. This information was used for the main aim of this study,  
143 which attempted a development of a non-targeted metabolomic approach based on MALDI-  
144 FTICR MS. A screening on the performances of six MALDI matrices and 36 different  
145 conditions (sample/matrix ratio, with or without addition of acid) led to the selection of three  
146 optimal combinations which enabled a satisfying non-targeted metabolite detection.  
147 Moreover, a rigorous control of experimental parameters such as the laser power used for  
148 MALDI measurements enabled an improvement of mass accuracy without complex sample  
149 deposition, which was based on the dried droplet method. MALDI resulted a complementary  
150 technique, leading to a ~60% increase of detected metabolites at both low and at high *m/z*  
151 values. Matrix effects arising from increased salinity in ESI-FTICR MS and MALDI-FTICR  
152 MS mode were evaluated on desalted *P. sativum* RE samples which were spiked with  
153 increasing amounts of salts. Lastly, the optimized non-targeted metabolomic approach based

154 on MALDI was tested on a true lyophilized *P. sativum* RE sample containing a natural  
155 amount of salt arising from the exudation step.

156

## 157 **2. Material and methods**

### 158 **2.1 Collection of plant root exudates.**

159 Plant seeds were purchased from RAGT Semences (Toulouse, France). Seeds were cleaned  
160 and stored in containers at 5 °C in a cool room until use. Pea seeds were soaked twice for 10  
161 min in an ethanol solution (96%) and then in a hypochlorite solution (26 %) under stirring.  
162 After each immersion, the seeds were rinsed six times with demineralized sterile water (10 s  
163 per rinse). The disinfection process was carried out in sterile conditions. For germination,  
164 sterilized seeds of pea were cultivated in boxes with agar (1 %). The seeds were germinated in  
165 phytotronic chamber at a day/night cycle: 16 h, 23 °C / 8 h, 20 °C for a period of 7 days. After  
166 germination, seed were transferred in a hydroponic system containing ¼ Hoagland nutrient  
167 solution and cultured in a phytotronic chamber in the same condition as germination. A list of  
168 the oligo and micro elements with their concentration in the ¼ diluted Hoagland solution can  
169 be found in table 1S. Five weeks growth seedling characterized of 6-8 leaves each plant were  
170 used for exudation. Briefly, the plants roots were removed from the Hoagland solution and  
171 briefly rinsed with sterile deionized water to remove the remaining nutrient solution. The  
172 plants were then transferred to backers containing 500 mL sterile ultrapure water. Exudation  
173 was carried out for 1h, roots were then removed and the solutions frozen at -20°C in glass  
174 bottles. A blank solution was prepared using 500 mL sterile ultrapure water which was  
175 incubated in the similar conditions as backers of root exudates.

### 176 **2.2 Metabolites extraction.**

177 Two sample treatment methods were used for metabolites extraction and concentration.  
178 Desalted sample which contained an enriched fraction of *P. sativum* RE were obtained  
179 through solid phase extraction (SPE). Briefly, frozen *P. sativum* RE (500 mL) were  
180 completely thawed, distributed in tubes (Falcon) and solutions were centrifugated at low  
181 temperature (5°C) for 15 min at 10 000 rpm (Eppendorf 5804 R) in order to remove cell  
182 debris and eventual particles. Aliquots of supernatant liquid were collected to reach a final  
183 volume of 420 mL. Centrifuged RE solution were then submitted to SPE on an automated  
184 SPE WorkStation (6.25ws, Interchim France). A column filled with a hydrophilic modified

185 styrene-based polymer (PolyClean HLB, 3 mL x 200 mg, Interchim France) was used for the  
186 extraction of metabolites. The HLB column was washed prior to sample loading with 5 mL of  
187 methanol and 5 mL of water at a flow rate of 15 mL/min. RE were then passed through the  
188 activated polymeric cartridge at 3 mL/min. The polymeric phase was washed with 4 mL of  
189 LC-MS water at 3 mL/min and dried for 10 min using a gentle stream of nitrogen. Elution  
190 was then performed by passing through 3 mL methanol at 2 mL/min. Time spent for SPE  
191 extraction was around 3h for sample. The fraction was then dried completely under a nitrogen  
192 stream and resuspended in 250  $\mu$ L of water. Blank was treated likewise. Samples were kept at  
193 low temperature (5-7°C) during SPE and evaporation by soaking bottles in ice. This assured  
194 minimal degradation of metabolites during the time-consuming sample treatment. For  
195 lyophilized samples, sample treatment was similar, except that after centrifugation the final  
196 volume of 420 mL RE was distributed in clean tubes, frozen at -20°C for 24h and then  
197 lyophilized using a freeze dryer (BUCHI Lyovapor™ L-200). The lyophilized sample and a  
198 blank were resuspended both in 250  $\mu$ L of water. SPE and lyophilized samples were stored at  
199 -20°C until analysis.

### 200 **2.3 Sample preparation and DDA-MS measurements for metabolites annotation.**

201 *P. sativum* RE SPE extracts were thawed before analysis and solutions were directly  
202 submitted to DDA-MS without further treatment. The mass spectrometer was a hybrid  
203 quadrupole-time-of-flight instrument (QTOF, Synapt G2 HDMS, Waters MS Technologies,  
204 Manchester, UK) [86] coupled with an ultra-high-performance liquid chromatographic  
205 (UHPLC) system equipped with a diode array detector (Vanquish, Thermo Scientific, San  
206 Jose, CA, USA). The travelling wave ion mobility cell included in the instrument was not  
207 used during analysis. The column used for the elution was a reverse phase ACQUITY UPLC  
208 HSS T3 1.7  $\mu$ m of dimension 1.0 mm x 100 mm (Waters Manchester, UK) equipped with a  
209 0.2  $\mu$ m prefilter. The sample tray and column oven temperatures were set at 8 °C and 50 °C,  
210 respectively. The injection volume was set at 5  $\mu$ L for MS/MS measurements in positive  
211 mode and 10  $\mu$ L in negative mode. Flow rate of 0.100 mL/min was used. Mobile phase A  
212 consisted of water + 0.1 % formic acid and mobile phase B of acetonitrile + 0.1 % formic  
213 acid. The elution was the following: 0–2 min, 0% B; 2–3 min, 0–10% B; 3–10 min, 10–20%  
214 B; 10–14 min, 20–100% B; 14–17 min, 100% B; 17–18 min, 100–0% B; 18–25 min, 0% B.  
215 DDA-MS experiments were performed over a  $m/z$  50–1200 range in resolution mode  
216 (resolution 20 000 FWHM). A sodium formate solution was used for external calibration  
217 while a continuous lock mass correction was applied by infusing leucine enkephalin via the



218 LockSpray™ interface (reference scan frequency 10 sec, lock spray capillary 3.0 kV and cone  
219 voltage of 25 V in positive mode and respectively 10 s, 3.0 kV and 50 V in negative mode).  
220 Source in positive mode was operated as following: capillary 3 kV, sampling cone 25 V,  
221 extraction cone 5 V. The source temperature was 120°C, the cone gas flow and the  
222 desolvation gas flows were set respectively to 20 L/h and 600 L/h; desolvation temperature  
223 300 °C. For negative ion mode, parameters were the same excluded for the capillary which  
224 was set at 2.2 kV. Metabolites were fragmented automatically through a survey scan function  
225 when the precursor threshold peak intensity exceeded 1000 counts in positive mode and 800  
226 scans in negative mode. For each MS scan, the 3 most intense MS/MS ions were fragmented  
227 using 4 MS/MS scans accumulation. Then, each fragmented ion was excluded for 6 seconds  
228 with a scan time of 0.200 sec and an interscan time of 0.024 sec. Experiments were performed  
229 in the transfer cell which was filled with argon ( $6.10^{-3}$  mbar), using collision energy ranging  
230 from 10-20 eV for low  $m/z$  values to 10-30 eV for high  $m/z$  values. A linear variation was  
231 used along the whole range. The trap cell of the instrument was operated using a background  
232 collision energy of 4 eV.

233 For metabolites annotation, raw data were submitted to accurate mass measure on MassLynx  
234 (v. 4.2, Waters Corporation) and then converted in mzXML open format through the  
235 MSCConvert tool of ProteoWizard (v. 3.0.9992) using MS1 and MS/MS levels as filters. Raw  
236 data were then uploaded on the Global Molecular Networking Platform (GNPS,  
237 <https://gnps.ucsd.edu>) [87,88] and experimental spectra were queried against library search  
238 using the spectral library search in order to find possible matches. Ions corresponding to  
239 contaminants or matrix were subtracted automatically through the GNPS analysis. Metabolite  
240 annotation was performed on manual literature search for some abundant metabolites for  
241 which no match was found on GNPS databases.

242

#### 243 **2.4 Sample preparation and ESI-FTICR MS measurements.**

244 For ESI measurements, 100-fold diluted solutions in water/methanol (50/50, v/v) for both  
245 SPE and lyophilized samples were prepared. For measurements in positive ion mode, 0.1 %  
246 formic acid was added to the final diluted solution in order to favor protonated forms.  
247 Solutions were introduced directly in the electrospray source of a high-field FTICR mass  
248 spectrometer (SolariX MRMS, Bruker Bremen, Germany), equipped with a 12 T  
249 superconducting magnet and a dynamically harmonized ICR cell, in both positive and  
250 negative ion modes. Samples were introduced to the ion source through a syringe pump at a

251 flow rate of 90.0  $\mu\text{L min}^{-1}$ . Spectra were recorded at a transient length of 1.12 s (4 million  
252 points) with an accumulation time of 0.050 s in positive mode and 0.100 s in negative mode.  
253 A sodium trifluoroacetate solution at 0.1 mg/mL in acetonitrile/water (50/50, v/v) was used  
254 for external calibration by the acquisition of 30 accumulated scan spectra. Mass spectra were  
255 acquired over a  $m/z$  98–1500 range. A mass resolving power of around 700,000 at  $m/z$  200  
256 was achieved. A complete list of parameters used for ESI measurements can be found in  
257 Table 2S.

## 258 2.5 Sample preparation for MALDI-FTICR MS measurements

259 For MALDI measurements, six matrices were chosen among the most used in MALDI  
260 literature. These were: 2,5-Dihydroxybenzoic acid (DHB), alpha-Cyano-4-hydroxycinnamic  
261 acid ( $\alpha$ -CHCA), Sinapinic acid (ScA), trans-2-[3-(4-tert-Butylphenyl)-2-methyl-2-  
262 propenylidene] malononitrile (DCTB), 1,5-Naphthalenediamine (DAN) and 9-Aminoacridine  
263 (9-AA). Regarding matrix preparation: DHB and ScA were prepared at a concentration of 10  
264 mg/mL in water/methanol (50/50 v/v) and 9AA at a concentration of 9 mg/mL;  $\alpha$ -CHCA at  
265 10 mg/mL in MeOH/ACN (50/50 v/v), DCTB and DAN at 10 mg/mL in MeOH. The same  
266 solutions were prepared in duplicate and added of 0.1 % formic acid on the final volume. SPE  
267 and lyophilized samples were then mixed without further dilution with the seven matrices  
268 with a ratio sample:matrix of 1:1, 2:1 and 1:10. Then, for each mixture, two additional  
269 conditions were tested, namely with or without the addition of 0.1 % of formic acid (FA). The  
270 dried droplet method was used for sample deposition on a target plate (MTP 384 target plate  
271 ground steel BC, Bruker Daltonics, Germany) and for each sample, 5  $\mu\text{L}$  were deposited for  
272 each spot, on three different positions and samples gently dried under vacuum. For external  
273 calibration in positive mode, a mixture of the 3 peptides bradykinin, leucine enkephalin and  
274 angiotensin (each at a concentration of 10 pmol/ $\mu\text{L}$  in water) was prepared at a proportion  
275 1:1:1:3 with DHB at 10 mg/mL. In negative ion mode, a solution of 9-AA at 10 mg/mL was  
276 used for external calibration. For direct introduction MALDI-FTICR MS measurements, laser  
277 shots value was fixed to 200 for all matrices while laser power was optimized in order to  
278 reach a 10% ionization threshold. Laser power was set as follow: in positive mode for DHB at  
279 20, for  $\alpha$ -CHCA and DCTB at 14 and for ScA at 28. In negative mode for DCTB at 11, for  
280 DAN at 14 and for 9AA at 26. Values of the laser power were set as following for  
281 optimization in positive mode: for DHB at 12, 15, 17, 18, 20, 22, 24, 26; for  $\alpha$ -CHCA at 8, 9,  
282 10, 12, 13, 14, 15, 18; for ScA at 12, 15, 18, 19, 20, 22, 25, 27, 29, 32, 35, 37; for SA at 12,  
283 15, 18, 19, 20, 22; for DCTB at 6, 7, 8, 9, 10, 12, 15, 16 and in negative mode: for 9AA at 15,

284 17, 20, 23, 25, 27, 30 and 32; for DAN at 10, 13, 14, 15, 17 and for DCTB at 6, 8, 10, 11, 12,  
285 13 and 15. Curves fitted to sigmoid were obtained through the Boltzmann function on  
286 OriginPro 2018 (v. b9.5.0.193). Figure 1S shows the curves obtained for optimization of the  
287 laser power and the 10% threshold values for the investigated matrices. Except for source  
288 parameters, all other experimental parameters used to perform MALDI-FTICR MS  
289 measurements were set as in ESI-FTICR MS. These, together with additional parameters of  
290 the MALDI source, can be found in table 2S. Experimental design, parameters for internal  
291 calibration, molecular formula attribution and data visualization were performed accordingly  
292 to ESI-FTICR MS measurements.

## 293 **2.6 Sample preparation for salt tolerance evaluation**

294 In order to evaluate the salt tolerance of the two sources coupled with FTICR MS, series of  
295 solutions spiked with increasing amount of salts were prepared and injected in the instrument.  
296 ¼ diluted Hoagland solution was used for the evaluation as used nutritive solution for plant  
297 growth. For ESI-FTICR MS measurements, 100-fold diluted SPE solutions in water/methanol  
298 (50/50, v/v) were used, while for evaluation on MALDI-FTICR MS, the SPE solution with  
299 the DHB matrix 1:10 +0.1 % FA was the only investigated. Salt solution was added at a  
300 percentage of 0.01%, 0.05%, 0.1%, 0.5%, 1%, 5% and 10% on the final volume of the  
301 obtained solutions for ESI- and MALDI-FTICR MS. Measurements were performed in the  
302 two modes according to the experimental parameters used before and each acquisition was  
303 performed on 50 accumulated scans.

## 304 **2.7 Data analysis for ESI-FTICR MS and MALDI-FTICR MS measurements**

305 Following data acquisition, all data arising from both ESI- and MALDI-FTICR MS  
306 measurements were treated on Bruker Compass DataAnalysis software (v. 5.1). Each  
307 accumulated mass spectrum was peak picked (S/N 8), then mass calibration was confidently  
308 performed using a mass list of *Pisum Sativum* RE metabolites identified through DDA-MS  
309 (Table 3S). Standard deviation on  $m/z$  values determined after internal calibration on a set of  
310 34 points was found to be below 0.100 ppm using a linear fit. Spectra related to samples were  
311 subtracted of blanks in Xpose mode with ratio 5 and molecular formula were assigned on the  
312 subtracted spectra with the common boundaries: C<sub>1-50</sub>, H<sub>1-100</sub>, N<sub>1-8</sub>, O<sub>0-30</sub>, S<sub>0-1</sub> and P<sub>0-1</sub>.  
313 Attribution was performed considering M + H protonated forms and M + Na, K, Ca adducts  
314 for positive mode, while in negative mode only M – H forms were retained. Molecular  
315 formulas were assigned for peaks with relative intensity threshold of 0.2 %, within a *mSigma*

316 limit of 800 and a tolerance mass error of 0.1 ppm. RDBE limit were set from 0 to 80 and H/C  
317 ratio from 0 to 3. Data containing assigned formula were exported and manually handled to  
318 avoid molecular formula redundancy (molecular formula arising from protonated and adduct  
319 forms). Visualization of van Krevelen and double bond equivalent (DBE) plots were obtained  
320 through an in-house script. For ESI- and MALDI-FTICR MS, performance evaluation  
321 measurements for both 50 and 200 accumulated spectra were acquired in triplicate. For salt  
322 tolerance evaluation with the two sources triplicate analysis were acquired by accumulating  
323 50 spectra. Reduced time for analysis was used to limit major salt contamination of ESI  
324 source at high salt concentration.

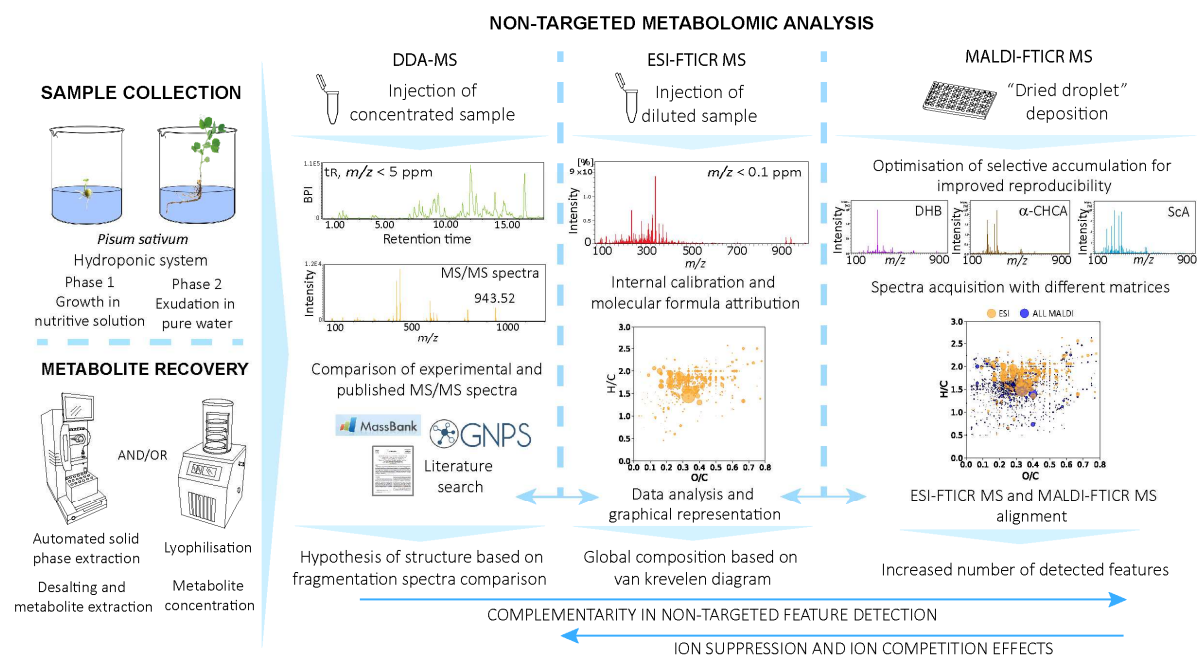
## 325 2.8 Solvents and reagents

326 All solvents and additives used to prepare mobile phases and sample solutions for ESI- and  
327 MALDI-FTICR MS measurements were LC-MS grade and they were purchased from Fisher  
328 Chemical (Pittsburgh, PA). 2,5 Dihydroxybenzoic acid, 9-aminoacridine and trans-2-[3-(4-  
329 tert-Butylphenyl)-2-methyl-2-propenylidene] malononitrile were at 98% purity. 1,5-  
330 Naphthalenediamine, sinapinic acid and sinapic acid were at 99% purity. All matrices were  
331 purchased from Sigma-Aldrich (Saint Luis, MO, USA). LC-MS grade formic acid used for  
332 sample acidification was purchased from Sigma-Aldrich (Saint Luis, MO, USA).

333

## 334 3. Results and discussion

335 Root exudates were submitted to preliminary DDA-MS and to ESI-FTICR MS analysis. This  
336 allowed to perform at first the annotation of major compounds based on the manual  
337 dereplication of fragmentation spectra and on the use of annotation tools as GNPS. Secondly,  
338 thanks to the van Krevelen diagram the global metabolic profile of *P. sativum* root exudates  
339 was obtained, highlighting the main chemical families. Once characterization performed with  
340 the two first techniques, sample were therefore subjected to MALDI-FTICR MS. The next  
341 paragraphs are dedicated to the description of the results with the different mass spectrometry  
342 platforms used for the analysis of RE. A summary of the analysis, annotation and  
343 interpretation workflow is showed in Figure 1.



344

345 *Fig. 1: Workflow used for the non-targeted metabolomic profiling of P. sativum root exudates*  
 346 *based on DDA-MS, ESI-FTICR and MALDI-FTICR complementarity*

347 **3.1 Identification of *Pisum sativum* root exudates based on DDA-MS measurements and**  
 348 **direct introduction ESI-FTICR-MS**

349 At first, DDA-MS measurements on *P. sativum* RE extracts obtained from SPE extraction  
 350 were performed in ESI positive mode through a hybrid QTOF mass spectrometer.  
 351 Experimental spectra were then submitted to literature manual search and database match on  
 352 the GNPS website. A list of metabolites for the 48 major compounds with proposed  
 353 annotation based on MS/MS spectra can be found in table 3S. The common metabolomic  
 354 annotation level was used to rank confidences in proposed metabolite structures [89]. The  
 355 compounds of interest belonged to seven molecular classes, namely nucleosides, amino acids,  
 356 fatty acids, fatty acid amides, alkaloids, oligopeptides, phosphocholines and triterpenes. In  
 357 addition to the main compound classes, other minor features presented fragmentation spectra  
 358 agreeing with polyphenols, glucosyl-phenols and indoles. In this study, on a total of 48, 34  
 359 features were annotated at level 2 of confidence and 14 features at a level 3. In fact, some of  
 360 the most intense metabolites detected via DDA-MS experiments did not found match with  
 361 literature or database search. For example, feature **19** at  $m/z$  367.1863 and molecular formula  
 362  $C_{18}H_{26}N_2O_6$  was detected together with two analogues and an isomer (features **23**, **25**, **27**)  
 363 which were separated through chromatography. The fragmentation spectrum (figure 2S)  
 364 presented two losses of 18 Da with fragment ions at  $m/z$  349.17  $[C_{18}H_{24}N_2O_5+H]^+$ ,  $m/z$  331.16

365  $[C_{18}H_{22}N_2O_4+H]^+$ , and fragments at lower  $m/z$  corresponding to  $m/z$  139.06  $[C_6H_6N_2O_2+H]^+$ ,  
366  $m/z$  121.04  $[C_6H_4N_2O+H]^+$  and  $m/z$  90.05  $[C_5H_4N_2+H]^+$ . These metabolites presented a  
367 fragmentation pathway similar to that of N-acyl homoserine lactones [90] and they were  
368 therefore annotated as fatty acid amides containing histidine or urocanate connected with a  
369 C18 or a C16 alkyl chain. Fatty acid amides, as N-acyl homoserine lactones, have been found  
370 to have an important role as *quorum sensing* molecules for bacteria communication and  
371 cooperation, especially in biofilm formation [91,92]. Moreover, it must be noted that histidine  
372 and urocanic acid (a product of histidine metabolism) are found at high concentration in the  
373 genus *Fabaceae*, which *P. sativum* belongs to, supporting the proposed annotation made for  
374 the fatty acid amides.[93]. Nonetheless, it must be noted that the fragmentation pathway  
375 showed some similarities with database spectra of some alkaloids as imidazole [94] or  
376 isoquinoline alkaloids [95]. Hence, this alternative annotation should not be excluded.  
377 Annotation as fatty acid amides was kept as the most trustable because the analyzed fraction  
378 showed the presence of many metabolites connected to lipid and lipid-like molecules. In this  
379 regard, our study pointed out on the presence of specialized metabolites, not yet isolated and  
380 discovered that can be a starting point for further research. The unambiguous identifications  
381 of the proposed metabolites should be performed through comparison of the experimental  
382 results with standard compounds or with complementary techniques as isolation and  
383 characterization through NMR. For many of the proposed metabolites, the biological role in  
384 *P. sativum* root exudation process as not been yet discovered, but according to published  
385 literature, *P. sativum* RE contain a high number of nitrogen-containing compounds with basic  
386 functional groups that are ionized preferentially in positive mode [96]. In fact, nitrogen  
387 compounds have been found to cover an important role in root-bacteria communication and  
388 ecosystem functioning. Metabolites for which a hypothesis of structure was formulated (Table  
389 3S) were used to create a list of reference compounds to be used as internal mass calibrants in  
390 ESI-FTICR MS measurements. Chemical classes were then used to gather the additional  
391 features detected through ultra-high-resolution mass spectrometry measurements and to  
392 discuss the differences in ionization *via* ESI- and MALDI-FTICR MS (next paragraphs).  
393 Once the first information on *P. sativum* RE obtained, 100-fold diluted RE SPE extracts were  
394 then submitted to ESI-FTICR MS analysis. Mass spectra of both samples and blanks acquired  
395 in positive mode accumulating 200 scans where then internally calibrated using a linear fit.  
396 The standard error over a  $m/z$  98-1500 range was lower than 0.100 ppm. After blank  
397 subtraction, molecular formulas were attributed for one analytical replicate according to the  
398 rules described in the materials and methods section. The wide diversity of heteroatoms (N, P,

399 S) and the presence of many adducts (Na, K and Ca) led often to multiple formula for each  
400 peak, especially for high  $m/z$  values in positive mode. No other adducts (Mg, Mn) resulted in  
401 preliminary formula assignment trials and they were therefore not considered. In general,  
402 when a double assignment was present, peaks were checked manually to remove unlikely  
403 molecular formula. This was performed when possible, based on the highest fit of the isotopic  
404 fine structure distributions for proposed formulas and experimental peaks. Conversely, the  
405 most logical formula based on the molecular classes that were found through DDA-MS  
406 experiments was retained. Nonetheless, it must be considered that different adducts could be  
407 present for the same molecule. For this reason, the obtained list was further cleaned up in  
408 order to reduce data redundancy and avoid that one molecule ionized in different forms (for  
409 example  $H^+$  form and  $Na^+$  form) could led to many different H/C ratios. Hence, molecular  
410 formulas of protonated forms were subtracted of a hydrogen and molecular formulas  
411 corresponding to Ca adducts were added of a hydrogen. Formula for K and Na adducts were  
412 kept unaltered. The list of molecular formula was then used to plot H/C ratios in function of  
413 O/C ratios and construct therefore the van Krevelen diagram (figure 3S) for ESI ionization.  
414 An in-house Python script was used for data visualization. As expected, an increase of the  
415 number of detected features was obtained thanks to ESI-FTICR MS measurements, with 486  
416 molecular formulas assigned in positive mode for the SPE sample. At our best, resulting  
417 annotation were submitted to PubChem search in order to propose insight on molecular family  
418 and subclasses. Figure 3Sa shows that *P. sativum* RE was characterized by a significant  
419 number of nitrogen-containing compounds, which consisted in a wide range of nucleosides  
420 and cytokines, amino acids and small oligopeptides, fatty acid amides, alkaloids and  
421 phosphocholines. Compounds that did not contain nitrogen or other heteroatoms were  
422 confirmed to be the triterpenes soyasaponins, a wide range of fatty acids that includes some  
423 plant hormones as jasmonic acid derivates or flavonoids. Among CHO compounds, a group of  
424 features that were not detected in DDA-MS had a molecular formula corresponding likely to  
425 glycolipids, which was taken as the best annotation. Moreover, thanks to the hypothesis of  
426 structures and information on the molecular families present in the sample, some  
427 unconventional molecular families were assigned for the first time to a definite zone of the  
428 van Krevelen diagram (Figure 3Sb). For example, it was possible to trace back the N-  
429 acylethanolamines at  $H/C = 2.0$  and  $O/C = 0.1$ , the fatty acid amides containing histidine or  
430 urocanic acid at  $H/C = 1.5$  and  $O/C = 0.3$  in a zone normally designed for oligopeptides, the  
431 soyasaponins glucosides at  $H/C = 1.6$  and  $O/C = 0.4$ . Similarly, oligopeptides at high N  
432 number ( $N=6$  or  $7$ ) were placed at  $H/C = 1.3$  and  $O/C = 0.2$  and glycolipids in an intermediate

433 zone between fatty acids and sugars, at  $H/C = 2$  and  $O/C = 0.5$ . The list of metabolites found  
434 through ESI-FTICR MS can be found in supplementary material. In general, all molecular  
435 formula for the compounds found through DDA-MS were found in their protonated or  $Na^+$ ,  
436  $K^+$  and  $Ca^{2+}$  adducts and were therefore confirmed through ESI-FTICR MS, giving a higher  
437 confidence level in metabolites annotation. Despite this, some compounds on a total of 48  
438 annotations were not found in ESI-FTICR MS spectra (table 3S). This could be due to the  
439 presence of residual salts or to an important number of ions that led likely to ion suppression  
440 and ion competition effects, despite the sample desalting through solid phase extraction. In the  
441 attempt to overcome these effects, experiments based on direct introduction MALDI-FTICR  
442 MS based on dried droplet deposition were performed and ionization in the two sources  
443 compared.

444

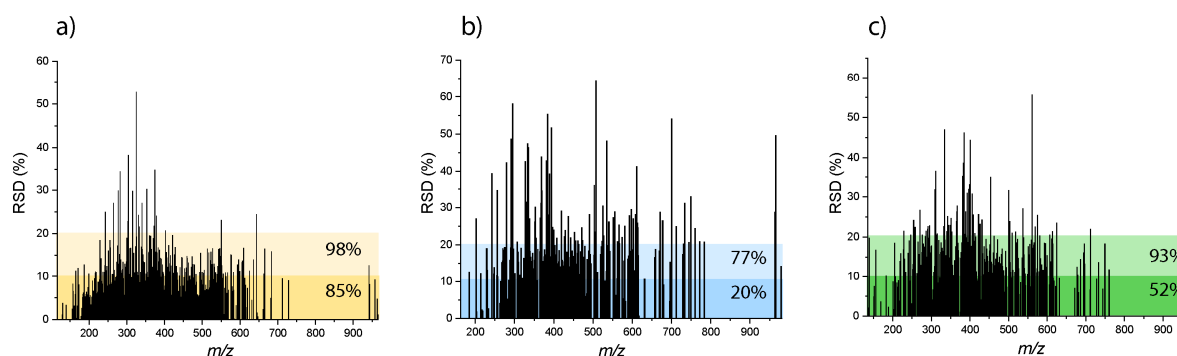
### 445 **3.2 Optimization of a direct introduction MALDI-FTICR-MS method for a non-** 446 **targeted metabolomic approach**

447 In ESI measurements samples are commonly injected with a constant flow by direct infusion.  
448 This translates likely in constant scan-to-scan ion abundance transmitted to the ICR cell, to  
449 reduced error on exact mass measurement and eventually, to good reproducibility of ion  
450 intensity in repeated measurements. In contrast, traditional MALDI sample preparation based  
451 on the “dried droplet” deposition has as main drawback an inhomogeneous distribution of  
452 analytes and matrices crystals in the deposited sample [62]. This represents a problem for  
453 quantitative analysis and, in the case of FTICR MS measurements, it can affect the  
454 reproducibility due to a change of scan-to-scan ion abundance transmitted to the ICR cell. In  
455 order to evaluate ESI and MALDI for a non-targeted metabolomic approach based on FTICR  
456 MS, repeatability was evaluated by calculating the relative standard deviation (RSD) on  
457 absolute signals intensity within three intra-day acquisitions of 50 accumulated scans for each  
458 mass spectrum. Results in ESI-FTICR MS mode obtained for *P. sativum* RE (SPE) samples  
459 showed that reproducibility of ion signals for the 85% of the features in the  $m/z$  range 98-1500  
460 was found appropriate, with deviation typically below 10%. Moreover, most metabolites  
461 showed RSD lower than 20% (Figure 2a). For the evaluation of reproducibility in intra-day  
462 MALDI-FTICR MS measurements on dried droplet deposited samples for non-targeted  
463 metabolomics, 50 scans accumulated spectra were first recorded without any supervision on  
464 the scan-to-scan ion abundance transmitted to the ICR cell during acquisition. Figure 2b  
465 shows the obtained RSD for MALDI features in unsupervised measurements: only 20% of the



466 features were found to have a 10% RSD and 77% below the 20%, while RSD up to 60%  
467 characterized a greater number of features. In order to minimize the variation of ion  
468 abundance in the ICR cell during the acquisition and to improve reproducibility in repeated  
469 measurements, an optimization of the selective accumulation was performed. 50 scans  
470 accumulated spectra were recorded using different ranges of selective accumulation. Selective  
471 accumulation allows to set a minimum (min) and a maximum (max) of intensity [97]. Mass  
472 spectra out of this range are discarded from the final average mass spectrum. Three ranges of  
473 selective accumulation were tested. A first range with min intensity  $5 \times 10^7$  and max  $5 \times 10^8$ , a  
474 second range at min  $1 \times 10^8$  and max  $5 \times 10^8$  and a third range at min  $1 \times 10^8$  and max  $3 \times 10^8$ .  
475 Figure 4S shows the profiles of accumulation on the total acquisition obtained from scan-to-  
476 scan total ion current entering in the ICR cell and considered for final spectrum, during a total  
477 of 50 scans. In general, more the range of selective accumulation was narrow, more the total  
478 ion current resulting from accumulation assumed a linear trend, reducing progressively the  
479 “wavy trends” corresponding to low signal accumulation scans, as showed in figures 4Sb and  
480 4Sc. Figure 4Sd shows that an ideal linear trend was obtained when selective accumulation  
481 spanned from a min of  $1 \times 10^8$  to a max of  $3 \times 10^8$  for each accumulated scan. It is worth to note  
482 that the lower limit influenced the signal threshold and its optimization allowed to discard  
483 acquisition scans corresponding to low density zone on the MALDI spot in which only signals  
484 of the noise were present. In this regard min value at  $5 \times 10^7$  led to the accumulation of spectra  
485 in which no signal corresponding to metabolites were present. While, the value of min  
486 selective accumulation equal set to  $1 \times 10^8$  allowed to obtain total ion signal in the mass  
487 spectra in the  $9 \times 10^6 - 1 \times 10^7$  range. Similarly, the optimization of the max limit avoided  
488 accumulation of too many ions in “hot spots”. It is worth to note that the overall scan-to-scan  
489 intensity with optimized ranges corresponded to an effective min intensity of  $1 \times 10^7$  to a max  
490 effective intensity of  $3 \times 10^8$  in mass spectra. This range corresponded to the intensity variation  
491 in one ESI mass spectrum, allowing a better comparison of final spectra acquired with the two  
492 ion sources. The optimization of the selective accumulation range resulted in the overall  
493 increase of mass spectra reproducibility and in a higher mass precision. In fact, RSD with  
494 MALDI reached satisfying values approaching results obtained with ESI. Figure 2c shows  
495 that with optimized ranges, 52% of metabolites had RSD below 10% and 93% in the 20%  
496 limit. Similarly, the standard error over a  $m/z$  98-1500 range was reduced from 0.150 ppm in  
497 the unsupervised analysis to 0.080 ppm using the optimized selective accumulation ranges  
498 These results represented an improvement towards a reliable analytical method based on  
499 classical deposition method for MALDI-FTICR MS applied to metabolomic analysis,

500 especially for the confident formula assignment in presence of high atomic diversity  
501 Nonetheless, it must be noted that, several scans were discarded yielding to an increase of  
502 analysis time up to 150%. For instance, for 200 accumulated scans, the run time was around 5  
503 min with unsupervised analysis and up to 12 to 15 min with the optimized selective  
504 accumulation range. Optimization was performed on a same spot containing DHB mix with  
505 the sample in proportion 1:10 + 0.1% FA. The laser power was optimized for all matrices in  
506 order to get comparable ionization thresholds, the optimized range of selective accumulation  
507 fitted with all other conditions.



508  
509 *Fig. 2: Relative standard deviation of signal intensity calculated for common metabolites on*  
510 *n=3 replicates found in Pisum Sativum RE for a) direct introduction ESI-FTICR MS, b)*  
511 *MALDI-FTICR MS without optimization of the selective accumulation and c) MALDI-FTICR*  
512 *MS under optimized conditions laying in a selective accumulation range of  $min=1\times 10^8$  and*  
513  *$max=3\times 10^8$ .*

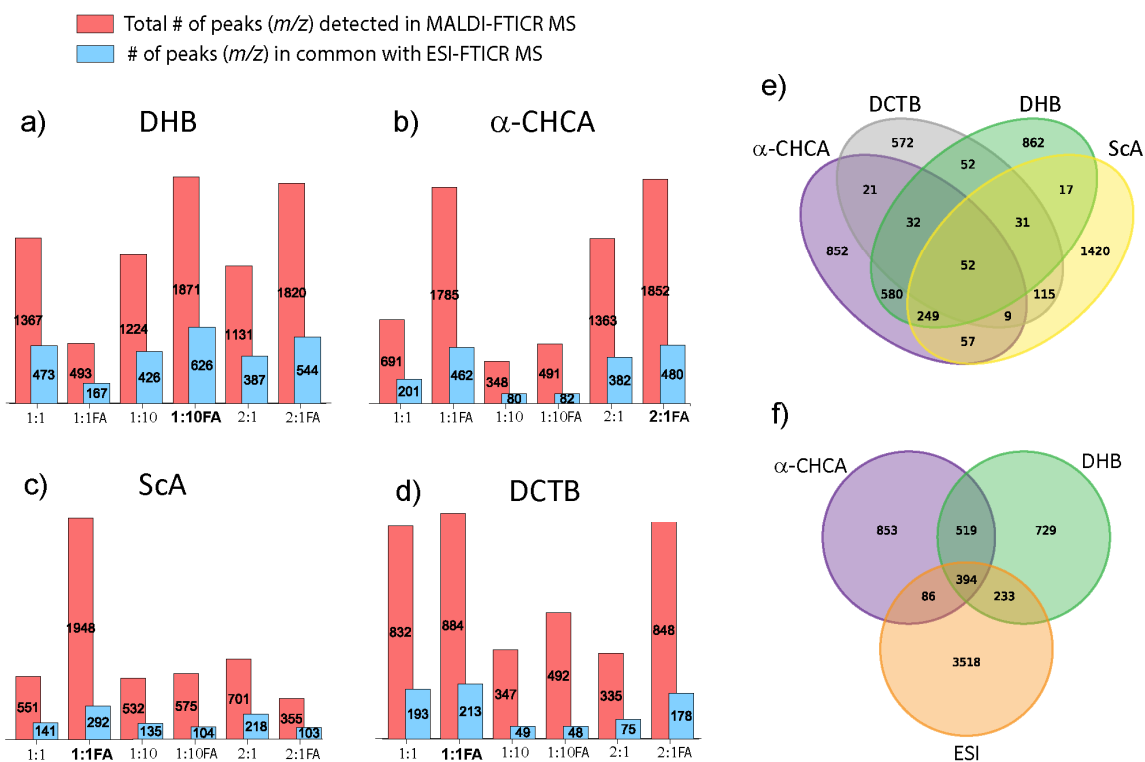
514

### 515 3.3 Evaluation of the efficiency of different MALDI matrices

516 In order to perform MALDI-FTICR MS analysis in best conditions for non-targeted  
517 metabolomic aims, an optimization of the most suited sample/matrix combination was  
518 performed. *P. sativum* RE SPE samples were mixed with the 6 matrices selected in this study  
519 at a ratio 1:1, 2:1 and 1:10. As ESI-FTICR MS measurements in positive mode were  
520 performed on acidified solutions to favor protonated forms against  $Na^+$  and  $K^+$  adducts, the  
521 three sample/matrix ratio for each matrix were also tested with the addition of 0.1% FA. For  
522 negative mode, the mixtures sample/matrix were used without any further addition. Solutions  
523 were deposited using the “dried droplet” method, dried under vacuum and analyzed through  
524 MALDI-FTICR MS. Mass spectra for the 24 conditions in positive mode and nine conditions  
525 in negative mode were acquired using the optimized selective accumulation range for 50

526 accumulated scans. Mass spectra were treated as previously described based on the three-steps  
527 procedure including internal calibration, blank subtraction and molecular formula assignment.  
528 The optimization of the best condition for each matrix was performed at an early stage of the  
529 study, the criteria for best condition selection was fixed to the higher number of common  $m/z$   
530 values found in ESI- and MALDI-FTICR MS spectra and on the highest number of features  
531 obtained in order to catch the maximum of detected features for a non-targeted metabolomic  
532 study (Figure 3). As alignment based on  $m/z$  values is performed before molecular formula  
533 assignment, isotopic peaks were counted in the total number of peaks. Nonetheless,  
534 comparative analysis for the different conditions could be still indicative of the best matrix  
535 conditions. For instance, among the six conditions tested for DHB, the ratio sample:matrix  
536 1:10 with the addition of 0.1% FA led to 626 common peaks with ESI-FTICR MS spectra and  
537 to a higher number of detected  $m/z$  values, while the other ratios using DHB were  
538 characterized by lower numbers. This led finally to select for further MALDI non-targeted  
539 metabolomic investigations in positive mode, the DHB matrix the ratio 1:10 + 0.1% FA, for  
540  $\alpha$ -CHCA the ratio 2:1 + 0.1% FA, for ScA and DCTB the ratio 1:1 + 0.1% FA. Moreover, an  
541 inspection of the histograms highlighted the presence of a relatively high number of peaks  
542 which were exclusively detected in MALDI spectra. These additional molecular formulas  
543 could arise both from the presence of multiple adducts formed and/or to additional  
544 metabolites for which detection was preferred in MALDI-FTICR MS mode (discussion in the  
545 next paragraph). Based on the number of common peaks, the global ionization of the sample  
546 in MALDI-FTICR MS was obtained in the order DHB >  $\alpha$ -CHCA > ScA > DCTB in positive  
547 mode. In fact, the ratio of common peaks on the total  $m/z$  detected in ESI-FTICR MS spectra  
548 (4231) was respectively 14.7%, 11.3%, 6.9% and 5%. Nonetheless, it must be considered that  
549 in presence of residual salts especially in ESI, the total  $m/z$  detected do not correspond  
550 necessarily to a corresponding number of unique features and that one compound may be  
551 present in form of multiple adducts.

552



553  
 554 *Fig. 3. Evaluation of the total number of peaks and the common peaks found in common with*  
 555 *ESI-FTICR MS spectra at different ratio sample/matrix for a) DHB, b)  $\alpha$ -CHCA, c) ScA and*  
 556 *d) DCTB in MALDI-FTICR MS spectra acquired in positive mode. Best ratios are highlighted*  
 557 *in bold style. Venn diagram obtained from alignment of  $m/z$  lists for the four selected*  
 558 *conditions (DHB 1:10 + 0.1% FA,  $\alpha$ -CHCA 2:1 + 0.1% FA, ScA and DCTB 1:1 + 0.1% FA)*  
 559 *and for the two highest ranked matrices (DHB 1:10 + 0.1% FA,  $\alpha$ -CHCA 2:1 + 0.1% FA)*  
 560 *with ESI-FTICR MS spectra are showed respectively in e) and f).*

561  
 562 This can explain the surprising low percentage found for common peaks in ESI- and MALDI-  
 563 FTICR MS spectra at this stage. A discussion on the number of common features obtained for  
 564 ESI and MALDI after molecular formula assignment is presented in the following paragraphs.  
 565 In general, a great conformity was found for all tested matrices, as the Venn diagram obtained  
 566 from alignment of the four best conditions showed the presence of many common  $m/z$  values,  
 567 even when two matrices of different chemical nature were compared. Only ScA was  
 568 characterized by a high number of additional peaks (1420) respect to ESI which were not  
 569 either in common with other matrices used in MALDI (Figure 3e). Nonetheless, DHB and  $\alpha$ -  
 570 CHCA obtained the highest score when compared with ESI and between the two, DHB  
 571 seemed to be the most appropriate for non-targeted metabolomics applications. It must be

572 noted that these results considered only the number of common peaks but did not take into  
573 account any information on the type of metabolites, on their intensity or on their detection in  
574 form of different adducts. All these concepts will be developed more in the following  
575 paragraphs.

576 MALDI in negative mode resulted in poor metabolites detection (Figure 5S) and low number  
577 of common features with ESI spectra (Figure 6S) in respect to positive mode (Figure 3). In  
578 fact, alignment in negative mode should be more indicative, as compounds were detected in  
579 ESI spectra preferentially as deprotonated forms, removing data redundancy experienced in  
580 positive mode. The best ratios sample / matrix were for 9AA 1:1, for DAN 2:1 and for DCTB  
581 1:1. In these conditions, the ratio of common peaks on the total of total  $m/z$  detected in ESI in  
582 negative mode (1987) was 5.2% for 9AA, 6% for DAN and 4.3% for DCTB. In conclusion,  
583 spectra in ESI negative mode were very informative and easy to study thanks to the absence  
584 of adducts. In comparison, MALDI negative mode did not bring substantial further  
585 information in the case of RE of *P. Sativum*. As a contrary, results in MALDI positive mode  
586 were highly complementary to the results in ESI positive mode. As a consequence, the  
587 negative mode in MALDI was not further investigated in this study and the following  
588 discussion will be focused on the non-targeted metabolomic approach in positive ion mode.  
589 Nonetheless, MALDI FTICR MS in negative mode should not be discarded *a priori* and  
590 further studies could be carried out with other matrices.

591

### 592 **3.4 Comparison of ESI-FTICR MS and MALDI-FTICR MS for non-targeted** 593 **metabolomics on *Pisum sativum* root exudates**

594 Once best conditions for MALDI ionization parameters and best ratios sample/matrix  
595 obtained, experiments were repeated for the selected conditions accumulating a higher  
596 number of spectra (200 accumulated scans). Measurements performed in triplicates were  
597 obtained from three different spots for each condition. Selected conditions for MALDI non-  
598 targeted metabolomics on *P. sativum* RE were for DHB analyte/matrix ratio of 1:10 and 0.1%  
599 FA, for  $\alpha$ -CHCA analyte/matrix ratio of 2:1 and 0.1% FA, for ScA analyte/matrix ratio of 1:1  
600 with 0.1% FA. Comparison was possible with ESI spectra as, scan-to-scan accumulation, total  
601 number of scans and final intensity resulted comparable (Figure 4S). Internal calibration,  
602 blank subtraction and molecular formula attribution were performed as previously stated.

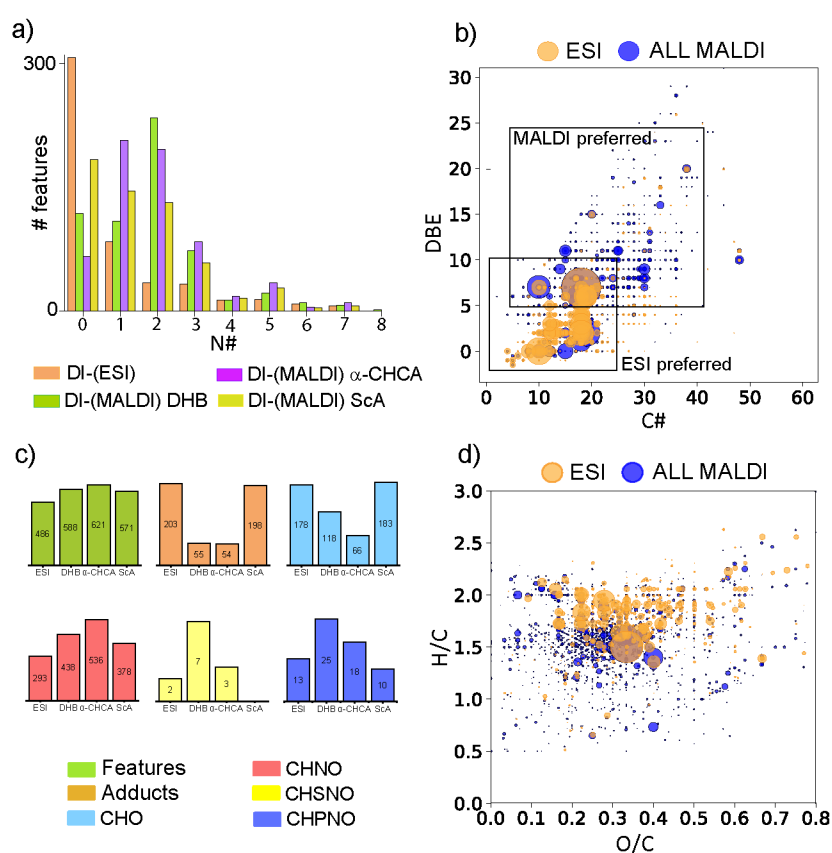
603 Figure 7S shows a comparison of the absolute intensity of selected features in ESI and  
604 MALDI with the three different matrices. The ionization efficiency towards six main families

605 were then compared. The six families were nucleosides (Figure 7Sa), amino acids and  
606 oligopeptides (7Sb), phosphocholines and phosphoserines (7Sc), fatty acids (7Sd), fatty acid  
607 amides containing histidine (7Se) and terpenes (7Sf). For each family, a number ranging from  
608 six to nine metabolites were selected according to the presence of a hypothesis of structure  
609 raising from DDA-MS measurements or, for assimilation to a chemical family, according to  
610 the molecular formula obtained from the ESI measurements. Error bars are relative standard  
611 deviation on the three replicates intensities obtained from three different spots. An analysis of  
612 the different chemical families allowed to retrieve the presence of particular ionization trends.  
613 For example, for all the studied nucleotides (Figure 7Sa), a better ionization yield was  
614 obtained in MALDI using  $\alpha$ -CHCA as matrix, with an increase of absolute intensity up to  
615 250% respect to the trace obtained in ESI. Conversely, DHB and ScA resulted less efficient in  
616 the ionization of nucleosides, leading to lower absolute intensities for the studied metabolites,  
617 when compared to ESI. For amino acids and oligopeptides (Figure 7Sb), the number of  
618 nitrogen atoms (N) in the molecule resulted crucial in the intensity yield. In fact, for low N  
619 number as for phenylalanine (Figure 7S-1b) or for oligopeptide with  $N \leq 4$  (Figure 7S-2b, -3b,  
620 -4b) ESI resulted in higher signal intensities, while MALDI with DHB matrix enabled a very  
621 efficient detection of features containing  $N \geq 5$ . Moreover,  $\alpha$ -CHCA led to higher absolute  
622 intensity for oligopeptides containing four to five N. In general, DHB was found to be the  
623 most suited matrix for oligopeptides with a signal increase respect to ESI up to 116 % and 85  
624 % respect to  $\alpha$ -CHCA. Fatty acids were preferentially ionized and detected in ESI (Figure  
625 7Sd). All fatty acids features were detected in MALDI, but at relatively low intensity.  
626 Triterpenes analyzed in the measurements included compounds as soyasaponin di-glucosides.  
627 Soyasaponins (Figure 7Sf) showed good ionization yield in MALDI with DHB matrix and in  
628 less extent also with  $\alpha$ -CHCA. Though, it must be noted that in ESI soyasaponins were  
629 ionized as protonated and Na adducts at comparable extent, while in MALDI, even with the  
630 addition of a 0.1% FA in the sample/matrix solution, the only adducts were the Na forms.  
631 Figure 7Sf shows therefore a comparison of intensity for Na adducts formed in the two  
632 sources. In the case of phosphocholines and phosphoserines (Figure 7Sc) and of fatty acid  
633 amides containing histidine (Figure 7Se), it was not possible to retrieve a global trend of  
634 ionization. For these chemical classes, preferential ionization seemed to be strongly dependent  
635 on the peculiar chemical structure. MALDI spectra obtained using ScA showed a preference  
636 for the ionization of oligopeptides, alkaloids and for some phosphocholines, but in general,

637 signals remained of poor intensity and showed therefore no major interest in non-targeted  
 638 metabolomic approaches.

639 In general, independently from the matrix, ionization in MALDI appeared to be preferred for  
 640 molecules containing high number of nitrogen atoms and to increase with the presence of  
 641 conjugate systems, as in the case of nucleotides. This hypothesis was first been made thanks  
 642 to rationalization of ionization yield for the metabolites annotated through DDA-MS  
 643 measurements. In order to deeply investigate this aspect, after molecular formula assignment,  
 644 the number of features (#) containing N atoms spanning from zero to eight was counted for  
 645 ESI and for MALDI with DHB,  $\alpha$ -CHCA and ScA and plotted as histogram (Figure 4a).

646



647

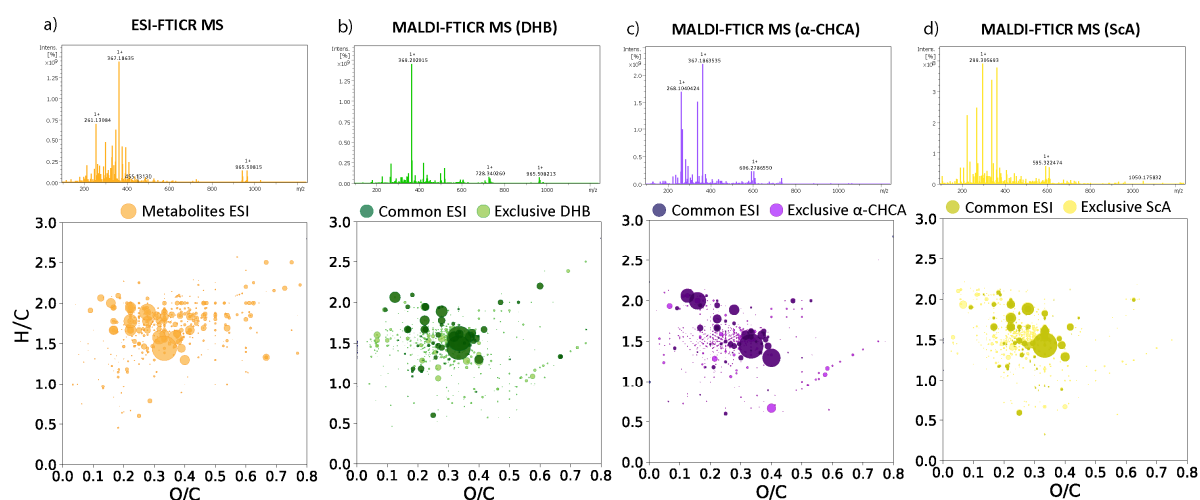
648 *Fig. 4: a) Histograms showing the number of detected features containing from one to eight*  
 649 *atoms of nitrogen in ESI (orange), MALDI DHB (green), MALDI  $\alpha$ -CHCA (purple) and*  
 650 *MALDI ScA (yellow); b) and d) show respectively the DBE vs #C plot and the van Krevelen*  
 651 *diagram obtained from molecular formula assignment of ESI (orange) and MALDI (blue)*  
 652 *obtained from the three matrices (DHB,  $\alpha$ -CHCA and ScA) spectra; c) total number of*  
 653 *assigned molecular formulas (green) and adducts (orange) together with the distribution of*

654 features containing CHO (light blue), CHNO (red), CHNSO (yellow) and CHNPO (blue)  
655 atoms.

656  
657 The molecular formula assignment revealed that effectively an increase of the number of  
658 features containing N was obtained with MALDI even if intensity for low number of N atoms  
659 resulted lower than in ESI, as previously stated (Figure 7S). On the other side, number of  
660 oxygen atoms (O#) seemed to have less effects on ionization *via* MALDI (Figure 8S), and a  
661 more relevant increase of features containing O# from two to four could be experienced  
662 probably as mirror of a higher N# in the molecules. These results agreed with the trends of  
663 relative intensity (%) at different N# and O#, for which histograms are showed in figure 9Sa  
664 and 9Sb, respectively.

665 Moreover, the double bond equivalent (DBE) and the carbon number (C#) were calculated  
666 from each assigned molecular formula for both ESI and MALDI, gathering together all  
667 features obtained from the three matrices (all MALDI). The resulting plot in Figure 4b shows  
668 that effectively, additional features detected for the first time through MALDI were generally  
669 characterized by higher DBE, up to 25, which corresponded to oligopeptides with N from six  
670 to eight. This highlighted that, ionization for unsaturated and high N# molecules was  
671 preferred in MALDI while ESI resulted in the preferential ionization of lower DBE  
672 compounds. The presence of additional features appeared surprising because MALDI spectra  
673 were characterized by simpler profiles respect to ESI spectra, while the obtained van Krevelen  
674 diagram showed great similarity (Figure 5).

675



676  
677 Fig. 5: Mass spectra obtained in positive mode and related van Krevelen diagrams for *Pisum*  
678 *sativum* root exudates obtained from molecular formula assignment based on ultra-high-



679 resolution a) ESI-FTICR MS and MALDI-FTICR MS with b) DHB, 2,5-dihydroxybenzoic  
680 acid, c)  $\alpha$ -CHCA,  $\alpha$ -Cyano-4-hydroxycinnamic acid and d) ScA, Sinapinic acid for the SPE  
681 desalted *P. sativum* RE sample.

682  
683 This mirrored both low signals for some metabolites and both a lower number of Na<sup>+</sup>, K<sup>+</sup> and  
684 Ca<sup>2+</sup> adducts. In fact, after molecular formula attribution, most of the features found in  
685 MALDI corresponded to protonated forms, while adducts were much less represented (Figure  
686 4c). As an example, feature **35** at  $m/z$  211.1325, corresponding to molecular formula C<sub>12</sub>H<sub>18</sub>O<sub>3</sub>  
687 (Table 3S) and annotated *via* DDA-MS as the plant hormone jasmonic acid (annotation level  
688 2), was detected in ESI as Na<sup>+</sup>, K<sup>+</sup> and Ca<sup>2+</sup> adducts, while in MALDI only the protonated  
689 form was found. Together with additional features, spectra obtained with MALDI showed  
690 common metabolites with ESI. Nonetheless, because of wide differences in ionization, it was  
691 difficult to evaluate the correct number of metabolites successfully ionized in both sources (as  
692 protonated or adducts) and, counting only the protonated forms, for all matrices around 10%  
693 of features were found to be in common. A list of metabolites found in ESI, MALDI (DHB)  
694 and MALDI ( $\alpha$ -CHCA) can be found as supplementary material. Examples of additional  
695 features corresponding to potential metabolites which were detected for the first time in *P.*  
696 *sativum* RE thanks to MALDI were features at  $m/z$  152.056675 (C<sub>5</sub>H<sub>5</sub>N<sub>5</sub>O, proposed  
697 identification guanine),  $m/z$  156.076770 (C<sub>6</sub>H<sub>9</sub>N<sub>3</sub>O<sub>2</sub> proposed identification histidine),  $m/z$   
698 166.072361 (C<sub>6</sub>H<sub>7</sub>N<sub>5</sub>O proposed identification methylguanine). The increase in the number of  
699 metabolites detected in MALDI corresponded to small metabolites, but also to molecules with  
700 higher  $m/z$  that are consistent to triterpenes and oligonucleotides as features at  $m/z$   
701 328.284593 (C<sub>19</sub>H<sub>37</sub>NO<sub>3</sub>, proposed identification palmitoyl alanine),  $m/z$  455.351968  
702 (C<sub>30</sub>H<sub>46</sub>O<sub>3</sub>, proposed identification moronic acid) or  $m/z$  740.340207 (C<sub>39</sub>H<sub>45</sub>N<sub>7</sub>O<sub>3</sub>, proposed  
703 identification cyclo[His-Tyr-Tyr-Leu-Tyr]). Features that were exclusively detected in  
704 MALDI are highlighted in bold style in supplementary materials.

705 Figure 4d shows the van Krevelen diagram obtained from molecular formulas obtained using  
706 ESI and MALDI with all matrices. It is worth to note that additional features are not likely to  
707 come from MALDI in-source fragmentation as the laser power and the number of shots were  
708 optimized for each matrix/sample mixture in order to be just slightly above the matrix  
709 ionization threshold. Moreover, the presence of the same additional metabolites in the spectra  
710 obtained from two distinct matrices represents an additional proof of the selective detection in  
711 MALDI mode. Nonetheless, it should be considered that in non-targeted metabolomic, the  
712 different nature of the metabolites could lead to different behaviors of chemical classes in

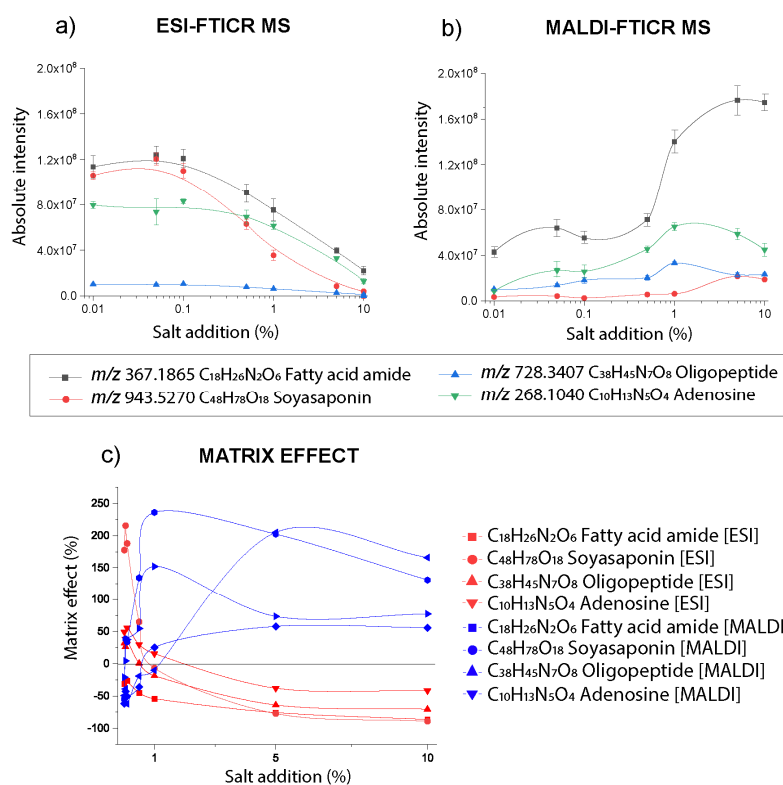
713 presence of the matrix, and a complete absence of fragmentation cannot be excluded *a priori*  
714 without further investigation. Anyway, results obtained herein shows that MALDI enabled a  
715 wide detection of compounds of different chemical classes, and it confirmed its potential as a  
716 complementary technique to ESI for a non-targeted metabolomic approach on biological  
717 samples.

718

### 719 **3.5 Salt tolerance and matrix effects in ESI and MALDI**

720 In order to evaluate salt tolerance of ESI and MALDI techniques for non-targeted  
721 metabolomics, mass spectra were recorded for a series of *P. sativum* RE SPE solutions which  
722 were spiked with various salt amounts. Indeed, in order to simulate the release of salts in  
723 hydroponic cultures, solutions were spiked with aliquots of Hoagland solution [98]. The last is  
724 a mixture of many salts for which the concentration is normally expressed in terms of  
725 electrical conductivity (EC, dS m<sup>-1</sup>), which depend on the metal content [99]. For example, ½  
726 Hoagland solution has EC of ~1.1 dS m<sup>-1</sup>, which for scale comprehension, corresponds to a  
727 concentration of ~ 10 mM NaCl, at pH=7 [100]. It is worth to note that, during the collection  
728 of the sample, a part of salts can be released together with the metabolites, but at any extent,  
729 the concentration should exceed the initial Hoagland EC used for plant growth. Series of  
730 solutions for measurements in the two sources were therefore prepared by adding a ¼  
731 Hoagland solution at 0.01%, 0.05%, 0.1%, 0.5%, 1%, 5% and 10% on the final sample. Salt  
732 ranges were chosen starting from a minimum equivalent salinity ~ 6 µM NaCl up to ~ 0.6 mM  
733 NaCl corresponding to the addition of 10% ¼ Hoagland solution. Measurements were  
734 performed in triplicates both for ESI and MALDI. For MALDI, the DHB matrix was selected  
735 because of its suitability for non-targeted metabolomic study as demonstrated before. In fact,  
736 even if α-CHCA led to higher intensity for many metabolites, DHB resulted in the  
737 simultaneous detection of many chemical classes. The variation of the absolute intensity of  
738 four case compounds belonging to different chemical classes, namely fatty acids,  
739 oligopeptides, soyasaponin triterpenes and nucleosides, at increasing salt concentrations is  
740 shown in Figure 6a for ESI and Figure 6b for MALDI.

741



742

743 *Fig. 6: Variation of the absolute intensity of four compounds of interest at increasing salt*  
 744 *concentrations in a) ESI and b) MALDI. Salt concentration is expressed in terms of % of the*  
 745 *Hoagland solution volume added to the sample (at log<sub>10</sub> scale). Matrix effect expressed as*  
 746 *[(I<sub>ME</sub>/I<sub>SPE</sub>)/I<sub>SPE</sub> × 100] in function of the salt addition for the four case metabolites in ESI and*  
 747 *MALDI are showed in panel c. Error bars calculated as standard deviation on three repeated*  
 748 *measurements are also shown.*

749 The protonated form for  $m/z$  367.1865 C<sub>18</sub>H<sub>26</sub>N<sub>2</sub>O<sub>6</sub> (annotated as fatty acid amide containing  
 750 urocanate),  $m/z$  728.3407 C<sub>38</sub>H<sub>45</sub>N<sub>7</sub>O<sub>8</sub> (annotated as an oligopeptide),  $m/z$  268.1040  
 751 C<sub>10</sub>H<sub>13</sub>N<sub>5</sub>O<sub>4</sub> (annotated as adenosine) and the sodium adduct for feature at  $m/z$  943.5270  
 752 C<sub>48</sub>H<sub>78</sub>O<sub>18</sub> (annotated as soyasaponin) were chosen for comparison of the two sources. Two  
 753 distinct trends were observed in the two sources with the increase of salt concentration. In  
 754 fact, while in ESI a ~ 6-fold signal drop was measured at salinity 10% for all compounds  
 755 (Figure 6a), the opposite trend was obtained in MALDI (Figure 6b). Not only the intensity  
 756 yield for all the ions remained mainly constant up to 0.5% Hoagland, but surprisingly, salts  
 757 addition had a positive matrix effect on ionization in the range 0.5%-5% leading to a  
 758 significant increase of the absolute intensity for all ions. Nonetheless, at Hoagland  
 759 concentration higher than 5%, salt tolerance in MALDI was the optimum while at higher  
 760 values the ion intensity decreased.

761 Nevertheless, the mere comparison of the absolute intensity for the case metabolites in the  
762 two sources can give only an idea on matrix effects at increasing salinity. For this reason,  
763 matrix effects in each source separately were further assessed by comparison of the peak  
764 intensity for the studied compounds in the spiked samples and in the starting SPE desalted  
765 sample which was used for salt tolerance. Matrix effect was then calculated according to  
766 Stahnke et al. [101] as:

$$767 \quad \text{Matrix effect (\%)} = \frac{I_{ME} - I_{SPE}}{I_{SPE}} \times 100$$

768  $I_{ME}$  is the intensity of a metabolite in the desalted SPE sample spiked with increasing salt  
769 amounts and  $I_{SPE}$  is the intensity of the same metabolite in the desalted SPE sample (with any  
770 addition of salts). The intensities were retrieved from the mass spectra obtained in ESI and  
771 MALDI for both desalted samples and spiked samples. In fact, assessment of matrix effects is  
772 usually performed using an analytical standard of known concentration analyzed in the same  
773 conditions. However, as concentration of the investigated compounds was not known in this  
774 study, the starting solution obtained through SPE before spiking was considered as a standard.  
775 It must be noted that this constituted an idealization as ion charge effects due to the sample  
776 complexity could influence as well the ionization of compounds in the SPE sample.  
777 Nonetheless, as the same SPE sample was used for spiking, the same complexity was kept  
778 into account when comparing spectra obtained with the same source. With the proposed  
779 formula, matrix effect values higher than 0 % described an increase of the signal in the spiked  
780 samples respect to the desalted sample, and therefore they were interpreted as signal  
781 enhancement. Similarly, values lower than 0 % denoted signal suppression. Figure 6c shows  
782 the obtained matrix effect (%) for four metabolites belonging to the different chemical classes  
783 in the two sources at increasing salinity. Signal suppression of around 50 % were obtained in  
784 ESI when passing from 0.01 to 1% salt concentration and at maximum salinity (10 % salts)  
785 matrix effect accounted to 70-80%. Contrarily, strong signal enhancements were obtained in  
786 MALDI with matrix effects accounting up to +150%. This mean that salt concentration equal  
787 to a 5% of the total sample volume would triple signal intensity for selected ions. Effectively,  
788 as signal enhancement obtained in MALDI resulted to be higher than signal suppression in  
789 ESI, it could be likely that for a same compound, a significative overtake of S/N in MALDI  
790 respect to ESI was experienced. It is worth to note that matrix effect does not affect all the  
791 compounds at the same extent. For example, in MALDI, metabolites with high N number as  
792  $m/z$  728.3407  $C_{38}H_{45}N_7O_8$  and  $m/z$  268.1040  $C_{10}H_{13}N_5O_4$  showed an absolute intensity drop  
793 already at 1% Hoagland concentration (Figure 6a). Ionization enhancement at high salt

794 concentration has been already showed in previous studies [102,103]and it has been explained  
795 as the result of the fast precipitation of salt crystals during evaporation respect to matrix-  
796 sample co-crystallization, which would decrease their location on the surface and favor their  
797 emplacement at the border of the spot. In the case of this study, ionization enhancement could  
798 be due to the peculiar nature of the Hoagland solution and the contained metals. In this extent,  
799 three different mechanisms can be considered : 1) the presence of a chelator in the Hoagland  
800 solution, namely EDTA (Table 1S), which would lead to the chelation of other metals and to  
801 their unavailability in forming adducts with the metabolites of the sample [104]; 2) the  
802 ionization of DHB matrix ions containing two aromatic carboxylic acid as adducts, which  
803 would reduce the ionization of matrix cluster and lead to an increase of solubility in water  
804 (contained in the RE sample and in less extent in the matrix solution), and eventually to a  
805 better analyte incorporation and homogeneity [105]; or 3) as already studied adducts can  
806 competitively binds with anionic analytes, favoring their desorption and reducing chemical  
807 noise [106].

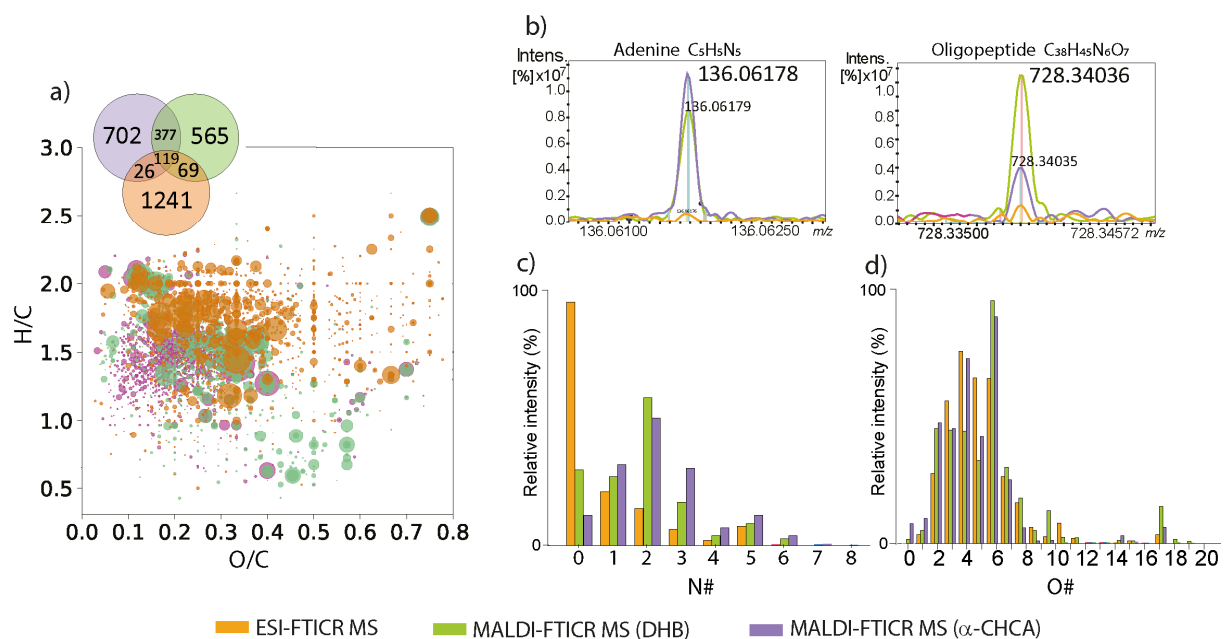
808 Likely, the improvement of the observed S/N for the metabolites in this study could be  
809 explained as the combination of the three factors.

810

### 811 **3.6 MALDI-FTICR MS applied to a true lyophilized *Pisum sativum* RE sample**

812 The proposed method based on MALDI for non-targeted metabolomic analysis of *P. sativum*  
813 RE has been optimized and evaluated on a metabolite fraction obtained through solid phase  
814 extraction. This constituted a simplified sample in which, together with metabolite extraction,  
815 a reduction of salts was performed. In most cases, solid phase extraction needs to be  
816 optimized for each sample and it represents a long and laborious process which is time-  
817 consuming. Moreover, together with salt elimination, the loss of the most polar metabolites  
818 can be experienced. As RE contain normally a high number of polar metabolites,  
819 lyophilization would lead to a less biased description of the real sample composition, at the  
820 expense of a higher salt concentration. For this reason, in order to evaluate the performances  
821 of the optimized non-targeted metabolomic approach based on MALDI on high salt  
822 concentration RE sample, measurements based on MALDI and on ESI were performed on a  
823 lyophilized *P. sativum* RE sample. Mass spectra were acquired, under the same experimental  
824 conditions previously used. From preliminary analysis, lyophilized samples resulted in a  
825 higher number of K<sup>+</sup> and Na<sup>+</sup> adducts, while Ca<sup>2+</sup> adducts represented sporadic cases. For this  
826 reason, Ca<sup>2+</sup> was not considered in molecular formula assignment. Repeatability evaluated by

827 aligning the list of  $m/z$  values extracted at relative intensity threshold higher than 0.2 %, led to  
 828 values of 80 % match for ESI, 78 % match for  $\alpha$ -CHCA, 76 % for DHB in MALDI  
 829 measurements. Molecular formulas were attributed accordingly to what was done for SPE  
 830 desalted samples.



831  
 832 Fig. 7: a) van Krevelen diagram obtained from formula assignment of ESI (orange), MALDI  
 833 with DHB (green) and  $\alpha$ -CHCA (violet) for *P. sativum* RE lyophilized samples. b) Overlap of  
 834 signals traces (ESI, orange; DHB, green;  $\alpha$ -CHCA, violet) for two  $m/z$  values corresponding  
 835 to case compounds which were detected only in MALDI. c) Relative intensity of features  
 836 containing from 1 to 8 atoms of nitrogen in ESI (orange), MALDI DHB (green), MALDI  $\alpha$ -  
 837 CHCA (violet) and MALDI ScA (yellow).

838 Figure 7a shows the van Krevelen diagram arising from formula assignment on spectra  
 839 obtained with the two sources for the lyophilized sample. As expected, a higher number of  
 840 assigned formulas was globally detected respect to the desalted sample obtained through SPE  
 841 (Figure 3a), highlighting that desalting led effectively to the loss of part of the metabolites.  
 842 Among these, a portion of features at O/C higher than 0.5 appeared, highlighting the recovery  
 843 of a higher proportion of polar metabolites. These molecules could correspond to nucleoside  
 844 phosphates, cyclic nucleotides, amino acids and glucoside flavonoids. The list of assigned  
 845 molecular formula for the lyophilized sample in ESI and in MALDI measurements with DHB  
 846 and  $\alpha$ -CHCA can be found as supplementary information. In general, molecular formula  
 847 assignment confirmed previous results, as a higher number of adducts was assigned in ESI  
 848 compared to MALDI spectra also for the lyophilized sample (Figure 10Sa).

849 Figure 7b shows the overlap of relative signal intensity obtained for two case metabolites in  
850 the two sources, namely  $C_5H_5N_5$  with  $[M+H]^+$  at  $m/z$  136.06178 annotated as adenine and  
851  $C_{38}H_{45}N_6O_7$  with  $[M+H]^+$  at  $m/z$  728.34036 annotated as an oligopeptide containing proline.  
852 While poor intensity signals for the two metabolites characterized ESI spectra, MALDI with  
853 both matrices led to higher S/N signals enabling their efficient detection and eventually,  
854 confident molecular formula assignment. Effectively, high salinity leading to ion suppression  
855 in ESI and ion enhancement in MALDI improved the detection of features in MALDI. This  
856 was especially valid for the DHB matrix that showed a strong signal enhancement compared  
857 to ESI. These findings agreed with the evolution of ion intensities at the increase of salt  
858 concentration presented in the previous paragraph (Figure 6) and allowed also to retrieve the  
859 approximative salinity, which was evaluated to be around 2 % (v/v) in lyophilized *P. sativum*  
860 RE. At this salt concentration, some metabolites were not detected in ESI but on average a  
861 higher number of detected features was obtained compared to MALDI (Figure 7a).  
862 Nonetheless, as previously stated, the total number of assigned formulas was redundant in ESI  
863 measurements because of the presence of several adducts. The Venn and van Krevelen  
864 diagrams were then plotted considering only the protonated forms in ESI and MALDI (Figure  
865 11S). In this case, similar plots were obtained, except for fatty acids and lipids ( $H/C=1.5-2$   
866 and  $O/C=0.1-0.3$ ), which showed to be the most affected from adduct formation (Figure  
867 10Sb). On the other side, a lower number of formulas only detected in ESI was obtained,  
868 keeping the number of common formulas almost unchanged (Figure 10Sb). Trends of relative  
869 intensity and number of detected features containing increasing N# and O# (showed  
870 respectively in figure 7d, 7d and 11Sa, 11Sb) confirmed results obtained for the SPE desalted  
871 sample. The two sources appeared to be highly complementary for a non-targeted  
872 metabolomic approach on root exudate samples. MALDI enabled an increase of detected  
873 features especially at relatively high salt concentration. Most of the metabolites exclusively  
874 detected with MALDI corresponded to nucleosides, alkaloids, flavonoids and highly aromatic  
875 compounds such as triterpenes and riboflavin analogues. For example, the exclusive detection  
876 in MALDI measurements was experienced for metabolites which molecular formula that  
877 could be tentatively assigned to quercetin analogues ( $m/z$   $C_{15}H_{10}O_7$ ), lumichrome ( $m/z$   
878  $C_{12}H_{10}N_4O_2$ ), lumiflavine ( $m/z$   $C_{13}H_{12}N_4O_2$ ), willardine ( $m/z$   $C_7H_9N_3O_4$ ) and anhydropisatine  
879 ( $m/z$   $C_{17}H_{12}O_5$ ). These molecules have a biological importance and they have been found to  
880 cover a principal role in *P. sativum* metabolism or to represent important mediators in plant  
881 growth and interaction with microorganisms [107–110].

882

883

#### 884 **4. Conclusion**

885 In this study, a non-targeted metabolomic approach *via* direct introduction MALDI-FTICR  
886 MS based on dried droplet deposition, was optimized on *P. sativum* root exudate samples.  
887 Optimized conditions of selective accumulation and best sample:matrix ratio for different  
888 matrices enabled improved precision and high metabolite cover up increasing the number of  
889 detected unique features compared to ESI-FTICR MS analysis. Moreover, matrix effect  
890 evaluation performed on RE spiked with salt showed the presence of ion suppression in ESI-  
891 FTICR MS and ion enhancement in MALDI-FTICR MS. Spectra obtained with MALDI were  
892 characterized by a lower complexity and led to an increase of detected unique features as a  
893 mirror of both lower number of adducts and preferential ionization of compounds at high N#  
894 and high DBE. Lyophilized root exudate samples analyzed through the two sources showed a  
895 good coverage of metabolite detection and annotation thanks to the ultra-high resolution, mass  
896 measure precision and dynamic range of FTICR MS, demonstrating that MALDI could be an  
897 alternative and complementary source for non-targeted metabolomics on biological samples.  
898 The authors believe that the results of this work are relevant in the field of non-targeted  
899 metabolomic and in the analysis of root exudate using a direct introduction approach based on  
900 FTICR MS. Moreover, the proposed method *via* direct introduction MALDI FTICR MS  
901 based on classic dried droplet deposition could be applied to other type of samples which are  
902 affected by matrix effects due to the presence of salts such as DOM and NOM in seawater,  
903 humic substances in fresh soil or in other biological samples as algae or blood. However,  
904 future works still require addressing some unresolved questions as for example, the  
905 optimization of an efficient MALDI FTICR MS method for RE analysis in negative mode or  
906 the research of new and more performant matrices for improved metabolite detection, sample  
907 homogeneity and high reproducibility for RE analysis. In this extent, solid-ionic or liquid-  
908 ionic matrices represent potential candidates for RE analysis through MALDI FTICR MS  
909 thanks to their co-crystallization properties and the possibility to be used both in positive and  
910 negative mode [111]. Moreover, future investigation should be dedicated also on defining the  
911 applicability and the limits of the optimized conditions found in this study on plants belonging  
912 to different genus and/or family or to study the RE changes in presence of rhizobacteria in the  
913 pursuit of a universal method based on MALDI FTICR MS for a comprehensive RE analysis.

914 **Author contribution: Valentina Calabrese:** Conceptualization, Data curation, Formal  
915 analysis, Investigation, Methodology, Visualization, Roles/Writing - original draft **Isabelle**



916 **Schmitz-Afonso:** Conceptualization, Funding acquisition, Project administration, Resources,  
917 Supervision, Validation, Writing - review & editing **Wassila Riah-Anglet:** Methodology,  
918 Writing - review & editing **Barbara Pawlak:** Funding acquisition, Project administration,  
919 Resources, Writing - review & editing **Isabelle Trinsoutrot -Gattin** Funding acquisition,  
920 Project administration, Methodology, Resources **Carlos Afonso:** Conceptualization, Funding  
921 acquisition, Project administration, Resources, Supervision, Validation, Writing - review &  
922 editing.

923 **Data availability** All the data are described within the manuscript. The raw data and metadata  
924 analyzed during the current study are available from the corresponding author on request.

925 **Acknowledgments** The authors gratefully acknowledge Pascal Cardinael (COBRA, Rouen,  
926 France) for the kind provision of the automatic SPE and Benjamin Pionnier (INTERCHIM,  
927 France) for support on its utilization. Anne Cauchois (UniLaSalle, Rouen, France) and Carole  
928 Burel (CURIB, Rouen, France) for advice in sample collection and sample treatment. Maxime  
929 Sueur, Oscar Lacroix-Andrivet and Julien Maillard (COBRA, Rouen, France) for the kind  
930 help and provision of the in-house script for FTICR data analysis. All the COBRA team for  
931 the support.

932

933 **Funding** This work was partially supported by Normandie Université (NU), the Région  
934 Normandie, the Centre National de la Recherche Scientifique (CNRS), Université de Rouen  
935 Normandie (URN), INSA Rouen Normandie, Labex SynOrg (ANR-11-LABX-0029), the  
936 graduate school for research XL-Chem (ANR-18-EURE-0020 XL CHEM), European  
937 Regional Development Fund (ERDF), Innovation Chimie Carnot (I2C) and SFR Normandie  
938 Végétal FED 4277. Financial support from Region Normandie and European Union (RIN  
939 Recherche Tremplin 2019 BEER) for conducting the research is gratefully acknowledged.  
940 Financial support from the IR INFRANALYTICS FR2054 for conducting the research is  
941 gratefully acknowledged. This work was supported the European Union's Horizon 2020  
942 Research Infrastructures program (Grant Agreement 731077).

943

944 **Declaration of competing interest** The authors declare that they have no conflict of interest.

945

946

947 **References**

- 948 [1] N. Vinayavekhin, A. Saghatelian, Untargeted metabolomics, *Curr. Protoc. Mol. Biol.*  
949 90.1 (2010)30–1 . <https://doi.org/10.1002/0471142727.mb3001s90>.
- 950 [2] A.C. Schrimpe-Rutledge, S.G. Codreanu, S.D. Sherrod, J.A. McLean, Untargeted  
951 Metabolomics Strategies—Challenges and Emerging Directions, *J. Am. Soc. Mass Spectrom.*  
952 27 (2016) 1897–1905. <https://doi.org/10.1007/s13361-016-1469-y>.
- 953 [3] W.B. Dunn, A. Erban, R.J.M. Weber, D.J. Creek, M. Brown, R. Breitling, T.  
954 Hankemeier, R. Goodacre, S. Neumann, J. Kopka, M.R. Viant, Mass appeal: Metabolite  
955 identification in mass spectrometry-focused untargeted metabolomics, *Metabolomics.* 9  
956 (2013) 44–66. <https://doi.org/10.1007/s11306-012-0434-4>.
- 957 [4] I. Nikolskiy, N.G. Mahieu, Y.J. Chen, R. Tautenhahn, G.J. Patti, An untargeted  
958 metabolomic workflow to improve structural characterization of metabolites, *Anal. Chem.* 85  
959 (2013) 7713–7719. <https://doi.org/10.1021/ac400751j>.
- 960 [5] A. Ribbenstedt, H. Ziarrusta, J.P. Benskin, 2018. Development, characterization and  
961 comparisons of targeted and non-targeted metabolomics methods, *PLoS One.* 13, e0207082.  
962 <https://doi.org/10.1371/journal.pone.0207082>.
- 963 [6] D.C. Sévin, A. Kuehne, N. Zamboni, U. Sauer, Biological insights through  
964 nontargeted metabolomics, *Curr. Opin. Biotechnol.* 34 (2015) 1–8.  
965 <https://doi.org/10.1016/j.copbio.2014.10.001>.
- 966 [7] M. Commisso, P. Strazzer, K. Toffali, M. Stocchero, F. Guzzo, 2013. Untargeted  
967 metabolomics: An emerging approach to determine the composition of herbal products,  
968 *Comput. Struct. Biotechnol. J.* 4, e201301007. <https://doi.org/10.5936/CSBJ.201301007>.
- 969 [8] C. Hu, J. Shi, S. Quan, B. Cui, S. Kleessen, Z. Nikoloski, T. Tohge, D. Alexander, L.  
970 Guo, H. Lin, J. Wang, X. Cui, J. Rao, Q. Luo, X. Zhao, A.R. Fernie, D. Zhang, Metabolic  
971 variation between japonica and indica rice cultivars as revealed by non-targeted  
972 metabolomics, *Sci. Rep.* 4 (2014) 1–10. <https://doi.org/10.1038/srep05067>.
- 973 [9] M.F. Turner, A.L. Heuberger, J.S. Kirkwood, C.C. Collins, E.J. Wolfrum, C.D.  
974 Broeckling, J.E. Prenni, C.E. Jahn, Non-targeted metabolomics in diverse sorghum breeding  
975 lines indicates primary and secondary metabolite profiles are associated with plant biomass  
976 accumulation and photosynthesis, *Front. Plant Sci.* 7 (2016) 953.  
977 <https://doi.org/10.3389/FPLS.2016.00953>.

- 978 [10] N. Schauer, A.R. Fernie, Plant metabolomics: towards biological function and  
979 mechanism, *Trends Plant Sci.* 11 (2006) 508–516.  
980 <https://doi.org/10.1016/J.TPLANTS.2006.08.007>.
- 981 [11] F.R. Castro-Moretti, I.N. Gentzel, D. Mackey, A.P. Alonso, Metabolomics as an  
982 Emerging Tool for the Study of Plant–Pathogen Interactions, *Metabolites*, 10 (2020) 52.  
983 <https://doi.org/10.3390/metabo10020052>.
- 984 [12] V. Vives-Peris, · Carlos De Ollas, · Aurelio Gómez-Cadenas, · Rosa, M. Pérez-  
985 Clemente, Root exudates: from plant to rhizosphere and beyond, *Plant Cell Rep.* 39 (2020) 3–  
986 17. <https://doi.org/10.1007/s00299-019-02447-5>.
- 987 [13] A. Canarini, C. Kaiser, A. Merchant, A. Richter, W. Wanek, Root exudation of  
988 primary metabolites: Mechanisms and their roles in plant responses to environmental stimuli,  
989 *Front. Plant Sci.* 10 (2019) 157. <https://doi.org/10.3389/fpls.2019.00157>.
- 990 [14] X. Zhang, R. Diao, X. Zhu, Z. Li, Z. Cai, Metabolic characterization of  
991 asthenozoospermia using nontargeted seminal plasma metabolomics, *Clin. Chim. Acta.* 450  
992 (2015) 254–261. <https://doi.org/10.1016/J.CCA.2015.09.001>.
- 993 [15] C.V. Carreño-Carrillo, E.V. Sánchez, C.V. Verduzco, J.E. Herbert-Pucheta,  
994 Polyphenol-based nuclear magnetic resonance non-targeted metabolomics of temperature-  
995 and time-controlled blue and red maize sprouting, *SN App. Sci.* 3 (2021) 1–10.  
996 <https://doi.org/10.1007/S42452-021-04171-W>.
- 997 [16] T. Koal, H.-P. Deigner, Challenges in Mass Spectrometry Based Targeted  
998 Metabolomics, *Curr. Mol. Med.* 10.2 (2010) 216–226.  
999 <https://doi.org/10.2174/156652410790963312>
- 1000 [17] P. Begley, S. Francis-McIntyre, W.B. Dunn, D.I. Broadhurst, A. Halsall, A. Tseng, J.  
1001 Knowles, R. Goodacre, D.B. Kell, Development and performance of a gas chromatography-  
1002 time-of-flight mass spectrometry analysis for large-scale nontargeted metabolomic studies of  
1003 human serum, *Anal. Chem.* 81 (2009) 7038–7046. <https://doi.org/10.1021/AC9011599>.
- 1004 [18] R. Díaz, H. Gallart-Ayala, J. v. Sancho, O. Nuñez, T. Zamora, C.P.B. Martins, F.  
1005 Hernández, S. Hernández-Cassou, J. Saurina, A. Checa, Told through the wine: A liquid  
1006 chromatography–mass spectrometry interplatform comparison reveals the influence of the  
1007 global approach on the final annotated metabolites in non-targeted metabolomics, *J*  
1008 *Chromatogr A.* 1433 (2016) 90–97. <https://doi.org/10.1016/J.CHROMA.2016.01.010>.

- 1009 [19] V. Calabrese, I. Schmitz-Afonso, C. Prevost, C. Afonso, A. Elomri, Molecular  
1010 networking and collision cross section prediction for structural isomer and unknown  
1011 compound identification in plant metabolomics: a case study applied to *Zhanthoxylum heitzii*  
1012 extracts, *Anal Bioanal Chem.* 1 (2022) 3. <https://doi.org/10.1007/s00216-022-04059-7>.
- 1013 [20] G.J. Patti, Separation strategies for untargeted metabolomics, *J Sep Sci.* 34 (2011)  
1014 3460–3469. <https://doi.org/10.1002/JSSC.201100532>.
- 1015 [21] B. Sarvin, S. Lagziel, N. Sarvin, D. Mukha, P. Kumar, E. Aizenshtein, T. Shlomi, Fast  
1016 and sensitive flow-injection mass spectrometry metabolomics by analyzing sample-specific  
1017 ion distributions, *Nat Commun.* 11 (2020) 1–11. <https://doi.org/10.1038/s41467-020-17026-6>.
- 1018 [22] H.A. Haijes, M. Willemsen, M. van der Ham, J. Gerrits, M.L. Pras-Raves, H.C.M.T.  
1019 Prinsen, P.M. van Hasselt, M.G.M. de Sain-Van der Velden, N.M. Verhoeven-Duif, J.J.M.  
1020 Jans, Direct Infusion Based Metabolomics Identifies Metabolic Disease in Patients' Dried  
1021 Blood Spots and Plasma, *Metabolites.* 9 (2019) 12. <https://doi.org/10.3390/metabo9010012>.
- 1022 [23] A. Aharoni, C.H.R. de Vos, H.A. Verhoeven, C.A. Maliepaard, G. Kruppa, R. Bino,  
1023 D.B. Goodenowe, Nontargeted Metabolome Analysis by Use of Fourier Transform Ion  
1024 Cyclotron Mass Spectrometry, *OMICS,* 6 (2002) 217–234.
- 1025 [24] A.G. Marshall, C.L. Hendrickson, G.S. Jackson, Fourier transform ion cyclotron  
1026 resonance mass spectrometry: a primer, *Mass spectrom rev.* 17 (2018) 1–35.  
1027 [https://doi.org/10.1002/\(SICI\)1098-2787\(1998\)17:1](https://doi.org/10.1002/(SICI)1098-2787(1998)17:1).
- 1028 [25] S.C. Brown, G. Kruppa, J.L. Dasseux, Metabolomics applications of FT-ICR mass  
1029 spectrometry, *Mass spectrom rev.* 24 (2005) 223–231. <https://doi.org/10.1002/MAS.20011>.
- 1030 [26] J. Han, R.M. Danell, J.R. Patel, D.R. Gumerov, C.O. Scarlett, J.P. Speir, C.E. Parker,  
1031 I. Rusyn, S. Zeisel, C.H. Borchers, Towards high-throughput metabolomics using ultrahigh-  
1032 field Fourier transform ion cyclotron resonance mass spectrometry, *Metabolomics.* 4 (2008)  
1033 128–140. <https://doi.org/10.1007/S11306-008-0104-8>.
- 1034 [27] P.M. Allard, G. Genta-Jouve, J.L. Wolfender, Deep metabolome annotation in natural  
1035 products research: towards a virtuous cycle in metabolite identification, *Curr Opin Chem*  
1036 *Biol.* 36 (2017) 40–49. <https://doi.org/10.1016/J.CBPA.2016.12.022>.

- 1037 [28] C. Roullier-Gall, M. Witting, D. Tziotis, A. Ruf, R.D. Gougeon, P. Schmitt-Kopplin,  
1038 Integrating analytical resolutions in non-targeted wine metabolomics, *Tetrahedron*. 71 (2015)  
1039 2983–2990. <https://doi.org/10.1016/j.tet.2015.02.054>.
- 1040 [29] M. Shahbazy, P. Moradi, G. Ertaylan, A. Zahraei, M. Kompany-Zareh, FTICR mass  
1041 spectrometry-based multivariate analysis to explore distinctive metabolites and metabolic  
1042 pathways: A comprehensive bioanalytical strategy toward time-course metabolic profiling of  
1043 *Thymus vulgaris* plants responding to drought stress, *Plant Sci*. 290 (2020) 110257.  
1044 <https://doi.org/10.1016/J.PLANTSCI.2019.110257>.
- 1045 [30] M. Maia, A. Figueiredo, C. Cordeiro, M. Sousa Silva, FT-ICR-MS-based  
1046 metabolomics: A deep dive into plant metabolism, *Mass Spectrom Rev*. (2021).  
1047 <https://doi.org/10.1002/MAS.21731>.
- 1048 [31] J.L. Wolfender, J.M. Nuzillard, J.J.J. van der Hoof, J.H. Renault, S. Bertrand,  
1049 Accelerating Metabolite Identification in Natural Product Research: Toward an Ideal  
1050 Combination of Liquid Chromatography-High-Resolution Tandem Mass Spectrometry and  
1051 NMR Profiling, *in Silico* Databases, and Chemometrics, *Anal Chem*. 91 (2019) 704–742.  
1052 <https://doi.org/10.1021/acs.analchem.8b05112>.
- 1053 [32] M.B. Comisarow, A.G. Marshall, The Early Development of Fourier Transform Ion  
1054 Cyclotron Resonance (FT-ICR) Spectroscopy, *J Mass Spectrom*. 31 (1996) 581–585.  
1055 [https://doi.org/10.1002/\(SICI\)1096-9888\(199606\)31:6](https://doi.org/10.1002/(SICI)1096-9888(199606)31:6).
- 1056 [33] F. Han, Y. Li, X. Zhang, A. Song, J. Zhang, R. Yin, Comparative study of direct  
1057 injection analysis and liquid chromatography mass spectrometry for identification of chemical  
1058 constituents in Kudiezi injection by FT-ICR MS, *Int J Mass Spectrom*. 405 (2016) 32–38.  
1059 <https://doi.org/10.1016/J.IJMS.2016.05.016>.
- 1060 [34] F. Han, Y. Li, X. Zhang, A. Song, H. Zhu, R. Yin, A pilot study of direct infusion  
1061 analysis by FT-ICR MS for rapid differentiation and authentication of traditional Chinese  
1062 herbal medicines, *Int J Mass Spectrom*. 403 (2016) 62–67.  
1063 <https://doi.org/10.1016/J.IJMS.2016.01.012>.
- 1064 [35] M. Gotthardt, B. Kanawati, F. Schmidt, S. Asam, R. Hammerl, O. Frank, T. Hofmann,  
1065 P. Schmitt-Kopplin, M. Rychlik, Comprehensive Analysis of the *Alternaria Mycobolome*  
1066 Using Mass Spectrometry Based Metabolomics, *Mol Nutr Food Res*. 64 (2020).  
1067 <https://doi.org/10.1002/mnfr.201900558>.

- 1068 [36] B.M. Ruddy, C.L. Hendrickson, R.P. Rodgers, A.G. Marshall, Positive Ion  
1069 Electrospray Ionization Suppression in Petroleum and Complex Mixtures, *Energ Fuel*. 32  
1070 (2018) 2901–2907. <https://doi.org/10.1021/acs.energyfuels.7b03204>.
- 1071 [37] K. Tang, J.S. Page, R.D. Smith, Charge competition and the linear dynamic range of  
1072 detection in electrospray ionization mass spectrometry, *J. Am. Soc. Mass Spectrom.* 15 (2004)  
1073 1416–1423. <https://doi.org/10.1016/J.JASMS.2004.04.034>.
- 1074 [38] A. Furey, M. Moriarty, V. Bane, B. Kinsella, M. Lehane, Ion suppression; A critical  
1075 review on causes, evaluation, prevention and applications, *Talanta*. 115 (2013) 104–122.  
1076 <https://doi.org/10.1016/J.TALANTA.2013.03.048>.
- 1077 [39] T.M. Annesley, Ion Suppression in Mass Spectrometry, *Clin Chem*. 49 (2003) 1041–  
1078 1044. <https://doi.org/10.1373/49.7.1041>.
- 1079 [40] R. Zenobi, R. Knochenmuss, Ion Formation In Maldi Mass Spectrometry, 17 (1999)  
1080 337–366. [https://doi.org/10.1002/\(SICI\)1098-2787\(1998\)17:5](https://doi.org/10.1002/(SICI)1098-2787(1998)17:5).
- 1081 [41] L.H. Cohen, A.I. Gusev, Small molecule analysis by MALDI mass spectrometry, *Anal*  
1082 *Bioanal Chem*. 373 (2002) 571–586. <https://doi.org/10.1007/S00216-002-1321-Z>.
- 1083 [42] K. Strupat, Molecular weight determination of peptides and proteins by ESI and  
1084 MALDI, *Methods Enzymol*. 405 (2005) 1–36. [https://doi.org/10.1016/S0076-6879\(05\)05001-](https://doi.org/10.1016/S0076-6879(05)05001-9)  
1085 9.
- 1086 [43] M. Levasseur, T. Hebra, N. Elie, V. Guérineau, D. Touboul, V. Eparvier,  
1087 Classification of Environmental Strains from Order to Genus Levels Using Lipid and Protein  
1088 MALDI-ToF Fingerprintings and Chemotaxonomic Network Analysis, *Microorganisms*. 10  
1089 (2022) 831. <https://doi.org/10.3390/microorganisms10040831>.
- 1090 [44] A.L. Yergey, J.R. Coorssen, P.S. Backlund, P.S. Blank, G.A. Humphrey, J.  
1091 Zimmerberg, J.M. Campbell, M.L. Vestal, De novo sequencing of peptides using  
1092 MALDI/TOF-TOF, *J. Am. Soc. Mass Spectrom.* 13 (2002) 784–791.  
1093 [https://doi.org/10.1016/S1044-0305\(02\)00393-8](https://doi.org/10.1016/S1044-0305(02)00393-8).
- 1094 [45] M. Barthélemy, V. Guérineau, G. Genta-Jouve, M. Roy, J. Chave, R. Guillot, L.  
1095 Pellissier, J.-L. Wolfender, D. Stien, V. Eparvier, D. Touboul, Identification and dereplication  
1096 of endophytic Colletotrichum strains by MALDI TOF mass spectrometry and molecular  
1097 networking, *Sci Rep*. 10 (2020) 1–16. <https://doi.org/10.1038/s41598-020-74852-w>.

- 1098 [46] C. Hao, X. Ma, S. Fang, Z. Liu, S. Liu, F. Song, J. Liu, S.-Y. Liu, Positive-and  
1099 Negative-ion Matrix-assisted Laser Desorption/Ionization Mass Spectrometry of Saccharides,  
1100 Rapid Commun. Mass Spectrom. 12 (1998) 345–348. <https://doi.org/10.1002/rcm.3072>.
- 1101 [47] C. Fenselau, F.A. Demirev, Characterization of intact microorganisms by MALDI  
1102 mass spectrometry, Mass Spectrom Rev. 20 (2001) 157–171.  
1103 <https://doi.org/10.1002/MAS.10004>.
- 1104 [48] H.Y. Wang, X. Chu, Z.X. Zhao, X.S. He, Y.L. Guo, Analysis of low molecular weight  
1105 compounds by MALDI-FTICR-MS, J Chromatogr B Analyt Technol Biomed Life Sci. 879  
1106 (2011) 1166–1179. <https://doi.org/10.1016/J.JCHROMB.2011.03.037>.
- 1107 [49] P. Champy, V. Guérineau, O. Laprèvote, molecules MALDI-TOF MS Profiling of  
1108 Annonaceous Acetogenins in Annona muricata Products for Human Consumption, Molecules.  
1109 14 (2009) 5235–5246. <https://doi.org/10.3390/molecules14125235>.
- 1110 [50] I.M. Taban, A.F.M. Altelaar, Y.E.M. van der Burgt, L.A. McDonnell, R.M.A. Heeren,  
1111 J. Fuchser, G. Baykut, Imaging of Peptides in the Rat Brain Using MALDI-FTICR Mass  
1112 Spectrometry, J Am Soc Mass Spectrom. 18 (2007) 145–151.  
1113 <https://doi.org/10.1016/j.jasms.2006.09.017>.
- 1114 [51] S.S. Dekeyser, K.K. Kutz-Naber, J.J. Schmidt, G.A. Barrett-Wilt, L.J. Li, N.C. Bird,  
1115 S.J. Atkinson, M.R. Clench, D. Mangnall, A.W. Majeed, M. Stoeckli, D. Staab, A.  
1116 Schweitzer, Y. Hsieh, R. Casale, E. Fukuda, J.W. Chen, I. Knemeyer, J. Wingate, R.  
1117 Morrison, W. Korfmacher, J. Chen, W.A. Korfmacher, S. Khatib-Shahidi, M. Andersson, J.L.  
1118 Herman, T.A. Gillespie, R.M. Caprioli, M.L. Reyzer, L. Signor, E. Varesio, R.F. Staack, V.  
1119 Starke, W.F. Richter, G. Hopfgartner, K.K. Kutz, L. Li, E.A. Stemmler, C.R. Cashman, D.I.  
1120 Messinger, N.P. Gardner, P.S. Dickinson, A.E. Christie, MALDI-FTICR Imaging Mass  
1121 Spectrometry of Drugs and Metabolites in Tissue, Anal Chem. 80 (2008) 5648–5653.  
1122 <https://doi.org/10.1021/AC800617S>.
- 1123 [52] B.A. Boughton, D. Thinagaran, D. Sarabia, A. Bacic, U. Roessner, Mass spectrometry  
1124 imaging for plant biology: a review, Phytochem Rev. 15 (2016) 445–488.  
1125 <https://doi.org/10.1007/S11101-015-9440-2>.
- 1126 [53] N.A. dos Santos, L.M. de Souza, F.E. Pinto, C.J. de Macrino, C.M. de Almeida, B.B.  
1127 Merlo, P.R. Filgueiras, R.S. Ortiz, R. Mohana-Borges, W. Romão, LDI and MALDI-FT-ICR

1128 imaging MS in: Cannabis leaves: Optimization and study of spatial distribution of  
1129 cannabinoids, *Anal Methods*. 11 (2019) 1757–1764. <https://doi.org/10.1039/c9ay00226j>.

1130 [54] N.A. dos Santos, C.M. de Almeida, F.F. Gonçalves, R.S. Ortiz, R.M. Kuster, D.  
1131 Saquetto, W. Romão, Analysis of Erythroxylum coca Leaves by Imaging Mass Spectrometry  
1132 (MALDI-FT-ICR IMS), *J Am Soc Mass Spectrom*. 32 (2021) 946–955.  
1133 <https://doi.org/10.1021/jasms.0c00449>.

1134 [55] K. Takahashi, T. Kozuka, A. Anegawa, A. Nagatani, T. Mimura, Development and  
1135 Application of a High-Resolution Imaging Mass Spectrometer for the Study of Plant Tissues,  
1136 *Plant Cell Physiol*. 56 (2015) 1329–1338. <https://doi.org/10.1093/PCP/PCV083>.

1137 [56] D. Veličković, V.S. Lin, A. Rivas, C.R. Anderton, J.J. Moran, An approach for broad  
1138 molecular imaging of the root-soil interface via indirect matrix-assisted laser  
1139 desorption/ionization mass spectrometry, *Soil Biol Biochem*. 146 (2020) 107804.  
1140 <https://doi.org/10.1016/J.SOILBIO.2020.107804>.

1141 [57] D. Veličković, R.K. Chu, G.L. Myers, A.H. Ahkami, C.R. Anderton, An approach for  
1142 visualizing the spatial metabolome of an entire plant root system inspired by the Swiss-rolling  
1143 technique, *J Mass Spectrom*. 55 (2020) e4363. <https://doi.org/10.1002/JMS.4363>.

1144 [58] S.A. Stopka, L.Z. Samarah, J.B. Shaw, A. v. Liyu, D. Veličković, B.J. Agtuca, C.  
1145 Kukolj, D.W. Koppenaal, G. Stacey, L. Paša-Tolić, C.R. Anderton, A. Vertes, Ambient  
1146 Metabolic Profiling and Imaging of Biological Samples with Ultrahigh Molecular Resolution  
1147 Using Laser Ablation Electrospray Ionization 21 Tesla FTICR Mass Spectrometry, *Anal*  
1148 *Chem*. 91 (2019) 5028–5035. <https://doi.org/10.1021/acs.analchem.8b05084>.

1149 [59] A. Onzo, R. Pascale, M.A. Acquavia, P. Cosma, J. Gubitosa, C. Gaeta, P. Iannece, Y.  
1150 Tsybin, V. Rizzi, | Antonio Guerrieri, R. Ciriello, G. Bianco, 2021. Untargeted analysis of  
1151 pure snail slime and snail slime-induced Au nanoparticles metabolome with MALDI FT-ICR  
1152 MS. *J Mass Spectrom*. 56 e4722. <https://doi.org/10.1002/jms.4722>.

1153 [60] A.N. Krutchinsky, B.T. Chait, On the nature of the chemical noise in MALDI mass  
1154 spectra, *J Am Soc Mass Spectrom*. (2002) 129–134. [https://doi.org/10.1016/S1044-](https://doi.org/10.1016/S1044-0305(01)00336-1)  
1155 [0305\(01\)00336-1](https://doi.org/10.1016/S1044-0305(01)00336-1).

1156 [61] C. Pan, S. Xu, H. Zhou, Y. Fu, M. Ye, H. Zou, Recent developments in methods and  
1157 technology for analysis of biological samples by MALDI-TOF-MS, *Anal. Bioanal. Chem*.  
1158 387 (2007) 193–204. <https://doi.org/10.1007/S00216-006-0905-4>



- 1159 [62] M.B. O'Rourke, S.P. Djordjevic, M.P. Padula, The quest for improved reproducibility  
1160 in MALDI mass spectrometry, *Mass Spectrom Rev.* 37 (2018) 217–228.  
1161 <https://doi.org/10.1002/MAS.21515>.
- 1162 [63] Y.N. Chai, D.P. Schachtman, Root exudates impact plant performance under abiotic  
1163 stress, *Trends Plant Sci.* 27 (2022) 80–91. <https://doi.org/10.1016/j.tplants.2021.08.003>.
- 1164 [64] V. Venturi, C. Keel, Signaling in the Rhizosphere, *Trends Plant Sci.* 21 (2016) 187–  
1165 198. <https://doi.org/10.1016/j.tplants.2016.01.005>.
- 1166 [65] T. Tian, A. Reverdy, Q. She, B. Sun, Y. Chai, The role of rhizodeposits in shaping  
1167 rhizomicrobiome, *Environ Microbiol Rep.* 12 (2020) 160–172. <https://doi.org/10.1111/1758-2229.12816>.
- 1169 [66] J. Sasse, E. Martinoia, T. Northen, Feed Your Friends: Do Plant Exudates Shape the  
1170 Root Microbiome?, *Trends Plant Sci.* 23 (2018) 25–41.  
1171 <https://doi.org/10.1016/j.tplants.2017.09.003>.
- 1172 [67] M.K. Hassan, J.A. McInroy, J.W. Kloepper, The Interactions of Rhizodeposits with  
1173 Plant Growth-Promoting Rhizobacteria in the Rhizosphere: A Review, *Agriculture* 142 (2019)  
1174 142. <https://doi.org/10.3390/AGRICULTURE9070142>.
- 1175 [68] A. Kumar, A. Dubey, Rhizosphere microbiome: Engineering bacterial competitiveness  
1176 for enhancing crop production, *J. Adv. Res.* 24 (2020) 337–352.  
1177 <https://doi.org/10.1016/j.jare.2020.04.014>.
- 1178 [69] N.M. van Dam, H.J. Bouwmeester, Metabolomics in the Rhizosphere: Tapping into  
1179 Belowground Chemical Communication, *Trends Plant Sci.* 21 (2016) 256–265.  
1180 <https://doi.org/10.1016/j.tplants.2016.01.008>.
- 1181 [70] E. Oburger, D.L. Jones, Sampling root exudates-Mission impossible?, *Rhizosphere*, 6  
1182 (2018) 116–133. <https://doi.org/10.1016/j.rhisph.2018.06.004>.
- 1183 [71] M. Escolà Casas, V. Matamoros, Analytical challenges and solutions for performing  
1184 metabolomic analysis of root exudates, *Trends Environ. Anal. Chem.* 31 (2021) e00130.  
1185 <https://doi.org/10.1016/J.TEAC.2021.E00130>.
- 1186 [72] V. Vranova, K. Rejsek, K.R. Skene, D. Janous, P. Formanek, Methods of collection of  
1187 plant root exudates in relation to plant metabolism and purpose: A review, *J. Plant. Nutr. Soil*  
1188 *Sci.* 176 (2013) 175–199. <https://doi.org/10.1002/JPLN.201000360>.

- 1189 [73] S. Hosseinzadeh, Y. Verheust, G. Bonarrigo, S. van Hulle, Closed hydroponic  
1190 systems: operational parameters, root exudates occurrence and related water treatment, *Rev.*  
1191 *Environ. Sci. Biotechnol.* 16 (2017) 59–79. <https://doi.org/10.1007/S11157-016-9418-6>.
- 1192 [74] J.E. Son, H.J. Kim, T.I. Ahn, Hydroponic systems, in: *Plant Factory: An Indoor*  
1193 *Vertical Farming System for Efficient Quality Food Production: Second Edition*, Elsevier  
1194 Inc., 2019, pp. 273–283.
- 1195 [75] C. Maucieri, C. Nicoletto, R. Junge, Z. Schmautz, P. Sambo, M. Borin, Hydroponic  
1196 systems and water management in aquaponics: A review, *Ital. J. Agron.* 13 (2018) 1–11.  
1197 <https://doi.org/10.4081/IJA.2017.1012>.
- 1198 [76] N. Sharma, N. Singh, Hydroponics as an advanced technique for vegetable production:  
1199 An overview Hydroponic View project Organic Farming View project, *J Soil Water Conserv.*  
1200 17 (2018) 364–371. <https://doi.org/10.5958/2455-7145.2018.00056.5>.
- 1201 [77] P. Dundek, L. Holík, T. Rohlík, L. Hromádka, V. Vranová, K. Rejšek, P. Formánek,  
1202 Methods of plant root exudates analysis: a review, *Acta Univ. Agric. Silvic. Mendel. Brun.* 59  
1203 (2011): 241–6.
- 1204 [78] Gransee A, Wittenmayer L. "Qualitative and quantitative analysis of water-soluble  
1205 root exudates in relation to plant species and development." *J. Plant. Nutr. Soil Sci.* 163  
1206 (2000): 381–385.
- 1207 [79] Y. Tsuno, T. Fujimatsu, K. Endo, A. Sugiyama, K. Yazaki, Soyasaponins: A New  
1208 Class of Root Exudates in Soybean (*Glycine max*), *Plant Cell Physiol.* 59 (2018) 366–375.  
1209 <https://doi.org/10.1093/PCP/PCX192>.
- 1210 [80] A. Evidente, A. Cimmino, M. Fernandez-Aparicio, A. Andolfi, D. Rubiales, A.  
1211 Motta, Polyphenols, Including the New Peapolyphenols A-C, from Pea Root Exudates  
1212 Stimulate *Orobanche foetida* Seed Germination, *J. Agric. Food Chem.* 58 (2010) 2902–2907.  
1213 <https://doi.org/10.1021/jf904247k>.
- 1214 [81] L.E. Makarova, L. v. Dudareva, I.G. Petrova, G.G. Vasil'eva, Secretion of Phenolic  
1215 Compounds into Root Exudates of Pea Seedlings upon Inoculation with *Rhizobium*  
1216 *leguminosarum* bv. *viceae* or *Pseudomonas* *siringae* pv. *lisi*, *Appl. Biochem. Microbiol.* 52  
1217 (2016) 205–209. <https://doi.org/10.1134/S0003683816020095>.

- 1218 [82] Y.-H. Kuo, F. Lambein, F. Ikegami, R. van Parijs, Isoxazolin-5-ones and Amino Acids  
1219 in Root Exudates of Pea and Sweet Pea Seedlings', *Plant Physiol.* 70 (1982) 1283–1289.  
1220 <https://academic.oup.com/plphys/article/70/5/1283/6078810>.
- 1221 [83] A. Evidente, M. Fernández-Aparicio, A. Cimmino, D. Rubiales, A. Andolfi, A. Motta,  
1222 Peagol and peagoldione, two new strigolactone-like metabolites isolated from pea root  
1223 exudates, *Tetrahedron Letters.* 50 (2009) 6955–6958.  
1224 <https://doi.org/10.1016/j.tetlet.2009.09.142>.
- 1225 [84] K. Yoneyama, X. Xie, H. Sekimoto, Y. Takeuchi, S. Ogasawara, K. Akiyama, H.  
1226 Hayashi, K. Yoneyama, Strigolactones, host recognition signals for root parasitic plants and  
1227 arbuscular mycorrhizal fungi, from Fabaceae plants, *New Phytol.* 179 (2008) 484–494.  
1228 <https://doi.org/10.1111/J.1469-8137.2008.02462.X>.
- 1229 [85] E. Foo, N.W. Davies, Strigolactones promote nodulation in pea, *Planta*, 234 (2011)  
1230 1073–1081. <https://doi.org/10.1007/s00425-011-1516-7>.
- 1231 [86] K. Giles, J.P. Williams, I. Campuzano, Enhancements in travelling wave ion mobility  
1232 resolution, *Rapid Commun. Mass Spectrom.* 25 (2011) 1559–1566.  
1233 <https://doi.org/10.1002/RCM.5013>.
- 1234 [87] J.S. Yu, L.F. Nothias, M. Wang, D.H. Kim, P.C. Dorrestein, K. bin Kang, H.H. Yoo,  
1235 Tandem Mass Spectrometry Molecular Networking as a Powerful and Efficient Tool for Drug  
1236 Metabolism Studies, *Anal. Chem.* 94 (2022) 1456–1464.  
1237 <https://doi.org/10.1021/ACS.ANALCHEM.1C04925>.
- 1238 [88] L.F. Nothias, D. Petras, R. Schmid, K. Dührkop, J. Rainer, A. Sarvepalli, I. Protsyuk,  
1239 M. Ernst, H. Tsugawa, M. Fleischauer, F. Aicheler, A.A. Aksenov, O. Alka, P.M. Allard, A.  
1240 Barsch, X. Cachet, A.M. Caraballo-Rodriguez, R.R. da Silva, T. Dang, N. Garg, J.M.  
1241 Gauglitz, A. Gurevich, G. Isaac, A.K. Jarmusch, Z. Kameník, K. bin Kang, N. Kessler, I.  
1242 Koester, A. Korf, A. le Gouellec, M. Ludwig, C. Martin H, L.I. McCall, J. McSayles, S.W.  
1243 Meyer, H. Mohimani, M. Morsy, O. Moyne, S. Neumann, H. Neuweger, N.H. Nguyen, M.  
1244 Nothias-Esposito, J. Paolini, V. v. Phelan, T. Pluskal, R.A. Quinn, S. Rogers, B. Shrestha, A.  
1245 Tripathi, J.J.J. van der Hooft, F. Vargas, K.C. Weldon, M. Witting, H. Yang, Z. Zhang, F.  
1246 Zubeil, O. Kohlbacher, S. Böcker, T. Alexandrov, N. Bandeira, M. Wang, P.C. Dorrestein,  
1247 Feature-based molecular networking in the GNPS analysis environment, *Nat. Methods.* 17  
1248 (2020) 905–908. <https://doi.org/10.1038/s41592-020-0933-6>.

1249 [89] L.W. Sumner, A.E. Alexander, A. Ae, D.B. Ae, M.H.B. Ae, R. Beger, C.A. Daykin,  
1250 A.E. Teresa, W.-M. Fan, A.E. Oliver, F. Ae, R. Goodacre, A.E. Julian, L. Griffin, A.E.  
1251 Thomas, H. Ae, N. Hardy, A.E. James, H. Ae, R. Higashi, A.E. Joachim, K. Ae, A.N.L. Ae,  
1252 J.C. Lindon, A.E. Philip, M. Ae, A.W.N. Ae, M.D. Reily, J.J.T. Ae, M.R. Viant, L.W.  
1253 Sumner, A. Amberg, D. Barrett, M.H. Beale, R. Beger, C.A. Daykin, Á.R. Higashi, R.  
1254 Higashi, O. Fiehn, R. Goodacre, Proposed minimum reporting standards for chemical analysis  
1255 Chemical Analysis Working Group (CAWG) Metabolomics Standards Initiative (MSI),  
1256 *Metabolomics*. 3 (2007) 211–221. <https://doi.org/10.1007/s11306-007-0082-2>.

1257 [90] A.M.S. Rodrigues, R. Lami, K. Escoubeyrou, L. Intertaglia, C. Mazurek, M. Doberva,  
1258 P. Pérez-Ferrer, D. Stien, Straightforward N-Acyl Homoserine Lactone Discovery and  
1259 Annotation by LC–MS/MS-based Molecular Networking, *J. Proteome Res.* 21 (2022) 635–  
1260 642. <https://doi.org/10.1021/acs.jproteome.1c00849>.

1261 [91] M. Teplitski, J.B. Robinson, W.D. Bauer, Plants secrete substances that mimic  
1262 bacterial N-acyl homoserine lactone signal activities and affect population density-dependent  
1263 behaviors in associated bacteria. *Mol. Plant Microbe Interact.* 13 (2000): 637–648.  
1264 <https://doi.org/10.1094/MPMI.2000.13.6.637>

1265 [92] S.C. Kim, K.D. Chapman, E.B. Blancaflor, Fatty acid amide lipid mediators in plants,  
1266 *Plant Sci.* 178 (2010) 411–419. <https://doi.org/10.1016/j.plantsci.2010.02.017>.

1267 [93] C. Vidal-Valverde, J. Frias, A. Hernández, P.J. Martín-Alvarez, I. Sierra, C.  
1268 Rodríguez, I. Blazquez, G. Vicente, Assessment of nutritional compounds and antinutritional  
1269 factors in pea (*Pisum sativum*) seeds, *J. Sci. Food Agric.* 83 (2003) 298–306.  
1270 <https://doi.org/10.1002/JSFA.1309>.

1271 [94] A.C.F. Sawaya, I.N. Abreu, N.L. Andreatza, M.N. Eberlin, P. Mazzafera, HPLC-ESI-  
1272 MS/MS of Imidazole Alkaloids in *Pilocarpus microphyllus*, *Molecules*, 13 (2008) 1518–1529.  
1273 <https://doi.org/10.3390/MOLECULES13071518>.

1274 [95] Z. Qing, Y. Xu, L. Yu, J. Liu, X. Huang, Z. Tang, P. Cheng, J. Zeng, Investigation of  
1275 fragmentation behaviours of isoquinoline alkaloids by mass spectrometry combined with  
1276 computational chemistry, *Sci Rep.* 10 (2020) 1–13. [https://doi.org/10.1038/s41598-019-](https://doi.org/10.1038/s41598-019-57406-7)  
1277 [57406-7](https://doi.org/10.1038/s41598-019-57406-7).

- 1278 [96] N. Sawatsky, R.J. Soper, A quantitative measurement of the nitrogen loss from the  
1279 root system of field peas (*Pisum avense* L.) grown in the soil, *Soil Biol. Biochem.* 23 (1991):  
1280 255–259.
- 1281 [97] J.S. Ramírez-Pradilla, C. Blanco-Tirado, M. Hubert-Roux, P. Giusti, C. Afonso, M.Y.  
1282 Combariza, Comprehensive Petroporphyrin Identification in Crude Oils Using Highly  
1283 Selective Electron Transfer Reactions in MALDI-FTICR-MS, *Energy Fuels.* 33 (2019) 3899–  
1284 3907. <https://doi.org/10.1021/ACS.ENERGYFUELS.8B04325>.
- 1285 [98] C.J. Asher, D.G. Edwards, Modern solution culture techniques, *Inorganic plant*  
1286 *nutrition*. Springer, Berlin, Heidelberg, (1983) 94–119.
- 1287 [99] U.C. Samarakoon, P.A. Weerasinghe, W.A.P. Weerakkody, Effect of Electrical  
1288 Conductivity [EC] of the Nutrient Solution on Nutrient Uptake, Growth and Yield of Leaf  
1289 Lettuce (*Lactuca sativa* L.) in Stationary Culture, *Acta Horticulturae*, 1266 (2019) 137–144.  
1290 <https://doi.org/10.17660/ActaHortic.2019.1266.19>.
- 1291 [100] S.H. van Delden, M.J. Nazarideljou, L.F.M. Marcelis, Nutrient solutions for  
1292 *Arabidopsis thaliana*: a study on nutrient solution composition in hydroponics systems, *Plant*  
1293 *Methods.* 16 (2020) 1–14. <https://doi.org/10.1186/S13007-020-00606-4>.
- 1294 [101] H. Stahnke, S. Kittlaus, nther Kempe, L. Alder, Reduction of Matrix Effects in Liquid  
1295 Chromatography–Electrospray Ionization–Mass Spectrometry by Dilution of the Sample  
1296 Extracts: How Much Dilution is Needed?, *Anal. Chem.* 84 (2011) 1474–1482.  
1297 <https://doi.org/10.1021/ac202661j>.
- 1298 [102] M. Dufresne, N.H. Patterson, J.L. Norris, R.M. Caprioli, Combining Salt Doping and  
1299 Matrix Sublimation for High Spatial Resolution MALDI Imaging Mass Spectrometry of  
1300 Neutral Lipids, *Anal. Chem.* 91 (2019) 12928–12934.  
1301 <https://doi.org/10.1021/ACS.ANALCHEM.9B02974>.
- 1302 [103] S. Xu, M. Ye, D. Xu, X. Li, C. Pan, H. Zou, Matrix with high salt tolerance for the  
1303 analysis of peptide and protein samples by desorption/ionization time-of-flight mass  
1304 spectrometry, *Anal. Chem.* 78 (2006) 2593–2599. <https://doi.org/10.1021/AC051572A>.
- 1305 [104] M. Bourdat-Deschamps, S. Leang, N. Bernet, J.J. Daudin, S. Néliu, Multi-residue  
1306 analysis of pharmaceuticals in aqueous environmental samples by online solid-phase  
1307 extraction-ultra-high-performance liquid chromatography-tandem mass spectrometry:  
1308 Optimisation and matrix effects reduction by quick, easy, cheap, effective, rugged and safe

1309 extraction, J. Chromatogr. A. 1349 (2014) 11–23.  
1310 <https://doi.org/10.1016/j.chroma.2014.05.006>.

1311 [105] J.M. Asara, J. Allison, Enhanced Detection of Phosphopeptides in Matrix-Assisted  
1312 Laser Desorption/Ionization Mass Spectrometry Using Ammonium Salts, *J. Am. Soc. Mass*  
1313 *Spectrom.* 10 (1999) 35–44.

1314 [106] I.P. Smirnov, X. Zhu, T. Taylor, Y. Huang, P. Ross, I.A. Papayanopoulos, S.A.  
1315 Martin, D.J. Pappin, Suppression of r-Cyano-4-hydroxycinnamic Acid Matrix Clusters and  
1316 Reduction of Chemical Noise in MALDI-TOF Mass Spectrometry, *Anal. Chem.* 76 (2004)  
1317 2958–2965. <https://doi.org/10.1021/ac035331j>.

1318 [107] F.D. Dakora, V.N. Matiru, A.S. Kanu, Rhizosphere ecology of lumichrome and  
1319 riboflavin, two bacterial signal molecules eliciting developmental changes in plants, *Front.*  
1320 *Plant Sci.* 6 (2015) 700. <https://doi.org/10.3389/fpls.2015.00700>.

1321 [108] F. Lambein, R. van Parijs, Isolation and characterization of 1-alanyl-uracil  
1322 (willardiine) and 3-alanyl-uracil (ISO-willardiine) from *Pisum sativum*." *Biochem. Biophys.*  
1323 *Res. Commun.* 32 (1968) 474–479. [https://doi.org/10.1016/0006-291X\(68\)90686-4](https://doi.org/10.1016/0006-291X(68)90686-4).

1324 [109] H. Kato-Noguchi, Isolation and identification of an allelopathic substance in *Pisum*  
1325 *sativum*, *Phytochemistry*, 62 (2003) 1141–1144. [https://doi.org/10.1016/S0031-](https://doi.org/10.1016/S0031-9422(02)00673-8)  
1326 [9422\(02\)00673-8](https://doi.org/10.1016/S0031-9422(02)00673-8).

1327 [110] S. Steinkellner, V. Lenzemo, I. Langer, P. Schweiger, T. Khaosaad, J.P. Toussaint,  
1328 H. Vierheilig, Flavonoids and Strigolactones in Root Exudates as Signals in Symbiotic and  
1329 Pathogenic Plant-Fungus Interactions, *Molecules*, 12 (2007) 1290.  
1330 <https://doi.org/10.3390/12071290>.

1331 [111] Armstrong, D.W., Zhang, L.K., He, L. and Gross, M.L., 2001. Ionic liquids as matrixes  
1332 for matrix-assisted laser desorption/ionization mass spectrometry. *Anal chem*, 73 (15) 3679–  
1333 3686. <https://doi.org/10.1021/ac010259f>

1334